Membrane potential dynamics of cerebellar nuclei neurons during eyeblink conditioning

Robin Broersen[1,2], Daniela Carulli[3,4], Cathrin B. Canto[1,2,#,*] and Chris I. De Zeeuw[1,2,#,*]

[1]Department of Cerebellar Coordination and Cognition, Netherlands Institute for Neuroscience, Royal Netherlands Academy of Arts and Sciences, 1105 BA, Amsterdam, The Netherlands

[2]Department of Neuroscience, Erasmus MC, 3015 CN, Rotterdam, The Netherlands

[3]Laboratory for Neuroregeneration, Netherlands Institute for Neuroscience, Royal Netherlands Academy of Arts and Sciences, 1105 BA, Amsterdam, The Netherlands

[4]Department of Neuroscience Rita Levi-Montalcini and Neuroscience Institute Cavalieri Ottolenghi, University of Turin, 10040, Turin, Italy.

[#]Correspondence: c.dezeeuw@erasmusmc.nl; c.canto@nin.knaw.nl

*Shared last authorship

Abstract

Learning to associate a cue with its aversive consequence enables animals to prevent harm. Associative conditioning relies on activity within the cerebellum, but little is known about how changes in synaptic inputs to its output neurons shape their membrane potential dynamics during learning. Here we studied these changes in inputs using whole-cell and juxtasomal recordings of cerebellar nucleus neurons in awake mice during eyeblink conditioning and doing post-learning structural analysis. We identified changes in mossy fiber- and Purkinje cell-, but not climbing fiber-, inputs, leading to changes in subthreshold processing that correlate with the level and direction of the conditioned eyelid movements. These changes appear sufficient, as optogenetic stimulation of the inputs evoke incremental eyelid closures over the course of conditioning. Our data reveal how electrophysiological and structural modifications at the level of synaptic inputs to cerebellar output neurons facilitate conditioning of eyelid movements.

Introduction

The brain has a remarkable ability to learn associations between repeatedly-occurring neutral and aversive stimulus pairs. A hallmark feature of associative learning during Pavlovian eyeblink conditioning (EBC) is the occurrence of conditioned eyelid movements (CRs) after repeated presentation of a neutral conditioned stimulus (CS) followed by an aversive unconditioned stimulus (US)[1,2]. The current working hypothesis is that the CS is at least partially conveyed to granule cells in

the cerebellar cortex by mossy fiber (MF) axons originating in the pontine nuclei (PN). Granule cells give rise to parallel fibers and innervate Purkinje cells (PCs). The US recruits climbing fibers (CFs) that powerfully excite PCs[3–5]. Both MFs and CFs have collaterals that innervate the cerebellar nuclei[6–10].

Key sites for plasticity during cerebellar learning are the parallel fiber to PC synapse[11–15] and the parallel fiber to molecular layer interneuron synapse[16,17]. Plasticity at these synapses, potentially in combination with intrinsic mechanisms[15,18] and structural changes of axonal fibers[19,20], leads to reductions in PC simple spike activity during the CS-US interval[3,16,21]. This in turn leads to disinhibition of the cerebellar nuclei neurons[22–24] as well as increased spiking activity of premotor and motor neurons downstream in the red nucleus and facial nucleus, respectively[25,26], thereby generating an eyelid movement. Within the complex of cerebellar nuclei (CN), the anterior interposed nucleus (IntA) and dorsolateral hump region (DLH) contain most eyeblink-encoding neurons[23,24,27]. Manipulating their activity disrupts both the acquisition and expression of CRs[28–30]. Furthermore, CRs remain partly intact after removal of the cerebellar cortex in fully conditioned mice[31], suggesting that part of the memory trace may be stored at the level of the nuclei[32]. However, in contrast to the synaptic plasticity mechanisms in the cerebellar cortex that contribute to eyeblink conditioning, those in the cerebellar nuclei remain largely obscure.

Here, we obtained *in vivo* whole-cell and juxtasomal recordings of IntA and DLH neurons in the CN of awake head-fixed mice during EBC to investigate the dynamics of their membrane potential in relation to learning. Both naive and conditioned CN neurons predominantly show excitatory post-synaptic potentials (EPSPs) in relation to the conditioned and unconditioned stimulus. The moment of occurrence of the EPSPs and the directionality of the resulting eyelid movements reverse during conditioning, with the EPSPs *following* eyelid openings in naive mice, but *preceding* the conditioned response (CR) in conditioned mice. Using linear discrimination analyses we show that synaptic as well as spike activity can successfully inform a decoder to distinguish CR versus no CR trials. The density of inputs from both the excitatory MFs and the inhibitory PC axons are increased during learning. Moreover, optogenetically stimulating MFs results in enhanced eyelid movements over the course of conditioning, highlighting how a synergy of electrophysiological and structural mechanisms at the level of the synaptic inputs to CN neurons can facilitate associative learning.

Results

To test our hypothesis that learning-induced changes in inputs to CN neurons alter membrane potential (V_m) dynamics we recorded from CN neurons in whole-cell mode during EBC in awake head-fixed mice on a treadmill (Fig. 1a). A green LED flash (CS) signaled the arrival of a corneal air puff (US) into the left eye 250 ms later and eyelid movements during the CS-US interval were used as a measure

of associative learning. Over the course of the acquisition mice showed robust associative learning (Supplementary Fig. 1a). Fully conditioned mice were subjected to a single session of *in vivo* whole-cell recordings in current-clamp mode, targeting the IntA and DLH regions (Fig. 1b). Identical recordings were also performed in mice naive to EBC. During recordings groups were presented with CS-US paired and CS or US unpaired trials and, as expected, performance of conditioned mice was significantly better than naive mice (Fig. 1c).

Membrane potential dynamics underlying CS-evoked eyelid movements

We obtained recordings from 8 and 6 CN neurons in conditioned and naive mice, respectively (Fig. 1d,e; Table 1). The percentage of neurons that responded to the CS with significant changes in V_m was higher in conditioned (n = 6; 75%) compared to naive mice (n = 2; 33.3%). Most neurons in conditioned mice showed excitatory post-synaptic potentials (EPSPs) and increased spike activity following the CS and US (n = 5; 83.3% of CS responders; Fig. 1e,f). One neuron showed inhibitory post-synaptic potentials (IPSPs) and reduced spike activity in response to the CS and the US, which was associated with the occurrence of CRs (Supplementary Fig. 2a,b). Some neurons also encoded spontaneous eyelid movements (Fig. 1d, arrowhead), confirming that we were indeed recording from eyelid-encoding CN neurons. *In vitro* recorded CN neurons can be classified into multiple cell-types[33,34], but classification based on *in vivo* electrophysiological properties alone appeared problematic[35,36] (Table 1). Since EPSPs were observed in most responding neurons and eyelid movements are at least partially driven by increased spike activity in excitatory projection neurons[25,33], we largely focused on EPSP neurons in our analysis.

Conditioned neurons showed an earlier EPSP onset during the CS-US interval (116.74 ± 6.79 ms after CS onset, n = 5 neurons) compared to naive animals (139.8 ± 32.08 ms, n = 2 neurons) (Fig. 1g). In conditioned neurons the EPSP peak occurred at 154.6 ± 9.24 ms after CS onset and maintained a depolarized plateau until US onset (Fig. 1f,g). Interestingly, some conditioned neurons showed an early EPSP peak after a rapid depolarization, possibly reflecting AMPA-mediated MF currents or synchronized PC disinhibition (Fig. 1f, arrowheads). In contrast, naive neurons showed a more transient depolarization with their EPSPs peaking at 178.6 ± 2.61 ms after CS onset. During CS-only trials, EPSP peak time in conditioned neurons occurred on average 308.8 ± 54.87 ms after CS onset (amplitude: 8.71 ± 2.02 mV); yet, these EPSPs were variable in duration (886.5 ± 260.36 ms) and half-width (207.1 ± 37.37 ms). Interestingly, across all trials the direction of the eyelid movements was opposite in the two groups in that conditioned mice showed classical CRs (eyelid closures; 10.35 ± 2.50 %UR), whereas naive mice showed eyelid openings (EOs; -7.87 ± 5.21 %UR).

Next, we compared EPSPs in CR positive (+) versus CR negative (-) trials in conditioned mice (Fig. 1h). For all neurons for which we recorded both CR+ and CR- trials we found that the EPSP amplitudes during CR+ trials (8.42 ± 3.32 mV) were higher than those during CR- trials (5.22 ± 3.53 mV), but at the group level this was not statistically significant ($P = 0.194$, paired t-test). Likewise, IPSP amplitudes were also larger on CR+ trials versus CR- trials (CR+: -8.73 ± 1.10, n = 17 trials; CR-: 1.30 ± 0.83, n = 39 trials, 1 neuron, $P < 0.001$, MWU test). To further investigate whether EPSP amplitudes are associated with eyelid amplitudes we performed a pooled correlation analysis across all trials in conditioned EPSP neurons, which revealed a significant positive correlation (Fig. 1i). Thus, larger eyelid movements are associated with larger EPSPs (Fig. 1i, Supplementary Fig. 2c). IPSP amplitudes were also significantly correlated with eyelid movements, but the data showed a clear segregation of trials with and without IPSPs, where IPSPs occurred preferentially on CR+ trials (Supplementary Fig. 2a,b,d). A correlation analysis for EPSP neurons in naive mice revealed that larger eyelid openings are also associated with larger EPSPs (Fig. 1j), especially when including only EO+ trials (Supplementary Fig. 2e). This shows that EPSPs scale with increasing eyelid movements in both naive and conditioned mice, regardless of eyelid direction.

Since CN neurons provide the cerebellar output to downstream eyelid-controlling motor areas, we hypothesized that V_m dynamics in conditioned mice precede CRs. In contrast, unconditioned EOs in naive mice may well be the result of cerebral cortical activity[37,38] and therefore occur later. Indeed, the V_m response in conditioned neurons started 44.05 ± 10.47 ms earlier than the CR (Fig. 1k). In contrast, the EPSP onset in naive neurons followed the EO onset by 40.21 ± 9.28 ms. These data suggest that CN neurons in naive mice encode a late efference copy of the command or feedback signal related to the EO, but not an early signal that generates the EO itself.

Spike activity during conditioned eyelid movements

We next investigated how EPSPs are converted into spike activity during EBC by performing juxtasomal loose-patch recordings in conditioned mice (Fig. 2a,b), which showed trials with and without CRs (Supplementary Fig. 1b). Out of 112 recorded neurons (average spike rate 72.97 ± 3.08 Hz, range 3.6-165.3 Hz), 50% of the neurons responded with significant changes in spike rate to the CS. 76.8% of these responders showed spike facilitation and 23.2% showed spike suppression, consistent with earlier data on CN spike activity during EBC[24]. Neurons that responded with spike facilitation to the CS showed on average significantly increased spike rates during CR+ trials (CR+: 48.22 ± 5.78, CR-: 31.12 ± 4.95, $P < 0.001$, Wilcoxon), while the timing of peak spike rate was comparable among CR+ and CR- trials (CR+: 202.6 ± 9.98, CR-: 176.2 ± 11.43, $P = 0.083$, Wilcoxon; Fig. 2c). We correlated the number of spikes during the CS-US period on CR+ trials with the CR amplitude across all spike facilitation

neurons and found, similarly to the V_m data, a significant correlation, indicating that larger eyelid closure coincides with more spikes (Fig. 2d).

Decoding of behavioral responses from V_m and spike data

To determine whether the eyelid response can be decoded from V_m trial data we performed linear discriminant analysis (LDA). V_m trial data, in which the spikes were removed, were pooled across all conditioned neurons (n = 8) and used to decode trials with and without a CR. The decoder performed significantly above chance level when including trials from all neurons and from CS-responding neurons (EPSP/IPSP), but not from EPSP neurons alone (Fig. 2e). The decoder thus performed best based on pooled EPSP and IPSP neuron traces combined. Strikingly, the time of peak decoding accuracy (125.2 ms after CS onset) coincided almost exactly with the onset of V_m dynamics (123.3 ± 8.03 ms after CS onset) and preceded the onset of CRs (160 ± 11.57 ms after CS onset) (Fig. 2f).

Next, we performed LDA on pooled spiking data from the juxtasomally recorded CN neurons. The decoder performed significantly above chance when including traces from all neurons or all CS-responders and best when including spike facilitation neurons only (Fig. 2g). However, decoding performance based on the spike data was worse than that based on V_m traces (Fig. 2i). Finally, in contrast to the decoding based on V_m traces, the best decoding based on spike data could be obtained with data later during the CS-US interval, *i.e.,* during the upward sloping phase of both the CR and average spike rate (Fig. 2h,j). These data are in line with the functional sequence of having the changes in subthreshold activity occurring prior to those of suprathreshold activity.

Encoding of the unconditioned stimulus in CN neurons

How do CN neurons encode the US? In contrast to the CS, the US mainly activates neurons in the inferior olive, which evoke complex spikes in PCs through CF activity[39]. CFs also have collaterals that innervate the CN[8,40], but it is unclear to what extent CN neurons integrate inputs from these collaterals. In our dataset, all conditioned and naive CN neurons showed significant V_m responses to the US (Fig. 3a). Neurons showing CS-evoked EPSPs also showed US-evoked EPSPs and the one neuron that showed CS-evoked IPSPs also showed US-evoked IPSPs (Supplementary Fig. 2a,b). Conditioned and naive mice had comparable US-evoked eyelid closure amplitudes (P = 0.105, independent t-test), EPSP amplitudes (P = 0.123, independent t-test) and EPSP half-widths (P = 0.201, Welch's t-test) (Fig. 3b-d). Amplitudes of US-evoked EPSPs were comparable to those of CS-evoked EPSPs (P = 0.461, unpaired t-test, US-evoked versus CS-evoked on CS-only trials, P = 0.808, unpaired t-test). We therefore pooled all US-only trial data from conditioned and naive mice and performed a correlation analysis between the normalized EPSP amplitude and eyelid amplitude. US-evoked eyelid closures

turned out not to be correlated with EPSP amplitudes (Fig. 3e), indicating that V_m encoding of the US does not change during conditioning and also does not scale with the US-evoked eyeblink.

Does a preceding CR influence encoding of the US in CS-US paired trials in conditioned mice? We separated CR+ and CR- trials and found similar US-evoked eyelid closures (P = 0.728, paired t-test), EPSP amplitudes (P = 0.997, paired t-test) and EPSP half-widths (P = 0.759, paired t-test) (Fig. 3f-i). In contrast, when we correlated the normalized CR amplitude and the US-evoked EPSP amplitude we found a weak, yet significant positive correlation (Fig. 3j), indicating that US-evoked EPSPs may be somewhat enhanced by preceding CRs. We corroborated this finding with our spiking data, in which 78.6% of the neurons responded to the US and 63.6% of these responders showed spike facilitation. Similarly to the V_m data, while spike rate amplitudes were comparable between CR+ and CR- trials (P = 0.135, Wilcoxon) (Fig. 3k), the number of spikes following the US was positively correlated with the CR amplitude (Fig. 3l). Together, we conclude that processing of US information in CN neurons may be influenced by preceding coding of CS-evoked information, but there is no direct evidence that V_m encoding of the US mediated by CF collaterals is altered.

Changes in mossy fiber and Purkinje cell inputs during conditioning

Does conditioning lead to structural changes in synaptic inputs onto CN neurons? To test this we subjected mice to 10 days of conditioning or pseudoconditioning (Supplementary Fig. 1c) and evaluated the expression of the vesicular glutamate transporters type 1 (VGLUT1) and type 2 (VGLUT2) in the IntA and DLH, both considered to be important eyeblink-encoding regions of the CN[30,41,42]. VGLUT1 and VGLUT2 can be used as markers for excitatory MFs and CFs, respectively, since CFs express only VGLUT2 and MFs can also express VGLUT1[43]. We found a significantly increased density of VGLUT1+ puncta in the DLH of the right hemisphere (contralateral to the air puff) of conditioned mice, but not in the left hemisphere (P = 0.018, ANOVA, cond. left vs right p = 0.031, Tukey; Fig. 4a,b). However, no significant change in VGLUT2+ puncta density was found in the DLH after conditioning (P = 0.678, ANOVA; Fig. 4a,c), while expression of neither VGLUT1 nor VGLUT2 was changed in the IntA after conditioning (P = 0.966, ANOVA; Supplementary Fig. 3a-c). These results suggest that VGLUT1+ MFs may be selectively increased in the right DLH during conditioning on the left side. How does this relate to our V_m recordings? Five out of seven EPSP CS-responder cells were recorded on the left side, but EPSP amplitudes between left and right appeared comparable (left: 6.11 ± 1.14 mV, right: 7.17 ± 2.65 mV).

We also investigated whether the inhibitory input to the CN changes at the structural level during conditioning by quantifying the expression of the postsynaptic protein Gephyrin as a marker for inhibitory synaptic connections[44,45] (Fig. 4d). Neurons with a soma size >250 μm^2 were selected as

putative glutamatergic neurons[34,46]. Gephyrin puncta densities in conditioned mice were comparable between the left and right DLH (P = 0.832, paired t-test) and therefore we pooled data from both sides of the CN. After conditioning the density of Gephyrin puncta in the DLH was significantly increased (Fig. 4e). In contrast, no significant change in Gephyrin puncta was observed in the IntA (P = 0.952, independent t-test; Supplementary Fig. 3d,e). To determine whether the increase in Gephyrin+ input to DLH may represent an increased density of PC terminals (~73% of all terminals) or other inhibitory connections[47], we quantified the percentage of Gephyrin+ puncta in DLH neurons that were not apposed to boutons of the calcium-binding protein calbindin D-28k (CALB) (Fig. 4f). CALB is expressed by PCs as well as by CFs[48,49], but only PC terminals are inhibitory. Therefore, Gephyrin+ puncta that are not apposed to CALB+ boutons represent inhibitory connections other than those provided by the PCs. We did not find a significant difference in the percentage of Gephyrin+/CALB- profiles (P = 0.431, MWT; Fig. 4g), indicating that the increase in Gephyrin puncta in DLH is probably due to an increase in PC terminals.

Simple spike activity of lobule HVI PCs is increased after conditioning

The increased density of VGLUT1+ MFs in the DLH after conditioning may suggest that conditioning is also facilitated by an overall increased MF drive to the cerebellar cortex. This could lead to an increased activity of eyeblink-encoding PCs in lobule simplex (HVI) at rest[50], while still preserving simple spike suppression during the expression of CRs[16]. We thereto reanalyzed a previous dataset[16] and found that PCs in conditioned mice exhibit higher spontaneous simple spike rates than those in the same lobule in naive mice (Fig. 4h,i). This global change in simple spike activity covered all PCs of the eyeblink region involved in that we did not observe any significant difference (P = 0.734, independent t-test) between the changes in the CR-responding and non-responding PCs in the conditioned mice (CR-responding: 97.7 ± 5.49 Hz, n = 26, non-responding PCs: 94.4 ± 8.13 Hz, n = 12). Instead, no significant difference (P = 0.698, independent t-test) in complex spike rate was observed between naive and conditioned PCs (cond: 1.25 ± 0.06 Hz, n = 38, naive: 1.21 ± 0.34 Hz, n = 17), consistent with the absence of increased VGLUT2+ CF terminals in the CN. Together, our results suggest that conditioning increases the MF drive of both the CN and the related part of the cerebellar cortex, ultimately resulting in higher baseline simple spike rates that may allow for a deeper suppression during CR expression[16].

Optogenetic stimulation of pontine nuclei neurons leads to larger eyelid movements after conditioning

Do the structural changes in VGLUT1+ MF inputs to lead to altered eyelid movements? To test this we measured eyelid movements evoked by optogenetic activation of pontine nuclei (PN) neurons over the course of conditioning. We expressed Chronos-GFP in the visual part of the lateral PN[51] and placed optic fiber implants directly above the PN (Fig. 5a). We observed GFP labeling in cells of the injected PN, as well as in labeled axons in the EB region of the CN and granule cell layer, indicative of effective transduction (Fig. 5b-d). Juxtasomal loose-patch recordings from CN neurons in the EB region of awake mice ~5 weeks after injections revealed that 75% of neurons showed changes in spike activity during optogenetic stimulation of the PN (Fig. 5e). Next, we conditioned injected mice for 10 days during which mice showed robust learning (Supplementary Fig. 1d). During the same acquisition period we recorded eyelid movements on day 0 (D0), day 5 (D5) and day 10 (D10), while providing optogenetic stimulation at the same intensity (Fig. 5f). We found that conditioned mice made larger short-latency optogenetically-evoked eyelid closures (< 150 ms) on D10 compared to D0 (Fig. 5g). Yet, the peak-time of eyelid closures remained unchanged (P = 0.214; RM ANOVA). Together, these results indicate that increases in VGLUT1+ MFs may be functionally relevant for controlling the amplitude, but not the timing, of CRs, as activation results in larger eyelid movements after conditioning.

Discussion

In this study we provide novel insights into the subthreshold neuronal encoding and plasticity mechanisms during cerebellar learning in the IntA and DLH, *i.e.,* the parts of the cerebellar nuclei that are crucial for both the acquisition and expression of conditioned EBC behavior[28–31,52–57]. We obtained *in vivo* whole-cell recordings of CN neurons in awake behaving mice to study the ongoing synaptic activity during EBC. We found that a larger proportion of CN neurons show V_m responses in conditioned than in naive mice, and that the EPSPs during the CS-US interval show differences between groups in that EPSPs in conditioned neurons start earlier and are sustained until US arrival. Yet, in both groups the EPSP amplitude was correlated with the amplitude and direction of eyelid movement with conditioned eyelid closures in conditioned mice and eyelid openings in naive mice. The finding that EPSP onset preceded CRs in conditioned mice suggests that CN neurons encode a CR motor command before the movement is initiated. In contrast, in naive mice EPSPs followed the onset of eyelid openings, suggestive of encoding an efference copy of the motor command. Eyelid openings may be initiated by activity in cerebral cortical areas[37,38].

To investigate how V_m dynamics are converted into spiking activity in CN neurons we analyzed juxtasomal recordings from CN neurons in addition to those obtained in whole-cell mode. During the

second half of the CS-US interval the increased spike responses in the spike facilitation cells coincided with the upward ramping phase of CRs. Interestingly, the upward ramping spike rate during CR+ trials is preceded by a sustained V_m depolarization until US arrival, which is in line with a potentially increased input from the MF collaterals as well as a reduced inhibition from PCs[3,16]. Both V_m and spike data could successfully inform a decoder to separate CR+ from CR- trials, where the onsets of V_m transients and the spiking activities during the last half of the CS-US interval were most informative, respectively. Accordingly, the time of peak decoding accuracy occurred at a much earlier time for V_m data compared to spike data. This suggests that considerable subthreshold synaptic activity precedes CN spike output and eyelid movements. Instead, conditioning does not alter the subthreshold representation of the US, other than that the amplitude of a preceding CR is slightly related to the size of the EPSP and the spike response after the US. Our data somewhat contrast with the finding that US-evoked activity in the dorsal accessory olivary nucleus diminishes over the course of conditioning[5852,59].

The findings on the electrophysiological changes of CN neurons during eyeblink conditioning were corroborated by those on the structural changes of their synaptic inputs from the glutamatergic MFs. Moreover, optogenetic stimulation of the PN neurons, the main source of MF input to the cerebellum, also elicited larger eyelid movements after conditioning, in line with the plastic effects of the MF output at the level of the CN neurons. Surprisingly, VGLUT1 expression increased significantly only on the contralateral side, which is at odds with the general notion that eyeblink-encoding neurons within the ipsilateral CN are supposed to be most relevant for conditioned behavior[6028,29,61]. On the other hand, our findings support previously observed learning-associated sprouting of MFs on both sides of the CN, with also a contralateral preponderance[20]. Possibly, the bilateral effects are part of the recently uncovered mechanism that local eyeblink conditioning can lead to more widespread defensive behavior, engaging multiple parts of the whole body[62].

The increased activity of the MFs probably also exerted global effects in the cerebellar cortex, as we observed that the PCs in conditioned mice showed a significantly higher spontaneous simple spike firing rate than those in the same eyeblink region in naive mice. The global character of this effect on the baseline activity was underscored by the finding that it occurred in both the CR-responding and non-responding PCs in the conditioned mice. Moreover, it may also explain why we observed an increase in the density of PC axon terminals in the CN, as higher neuronal activity may lead to structural expansion in general, including that of PCs[20,63]. For the eyeblink-encoding PCs this increased simple spike activity at rest might lead to a stronger dynamic impact of the simple spike suppression during the expression of the CRs[16,50,64,65]. Indeed, CN neurons, which are like PCs highly intrinsically active[24,35], are unusually sensitive to the differential impact of activity of PCs during

spontaneous behavior versus that during modulation[64]. In other words, to modulate CN activity to enhance a particular motor behavior, one can enhance the inputs of MF collaterals, but one can also alter the baseline simple spike activity of the PCs upstream. Interestingly, the current whole-cell and juxtasomal recordings of CN neurons during eyeblink conditioning as well as the post-hoc structural analyses support both mechanisms, highlighting that they may operate in a synergistic fashion.

Acknowledgements

We are grateful to the following people for their contribution to the study: J.W. Potters, H.J. Boele, S.K.E. Koekkoek, Z. Gao, M.M Ten Brinke, J.K. Spanke, A.C.H.G. IJpelaar, M. Tang, B. Winkelman, A. Court, C. Geelen, M. Mešković, G. Özel, M. Bouw, S.O. Stokman and M. Romijn. We thank I. Duguid and P. Chadderton for their constructive comments. This study was enabled by funding from Dutch Organization for Medical Sciences (ZonMw), Life Sciences (NWO), the ERC-advanced, CEREBNET and C7 programs of the European Community, INTENSE and DBI2 (C.I.D.Z.) as well as the Boehringer Ingelheim Fonds.

Author contributions

Conceptualization, R.B., C.B.C, C.I.D.Z.; Methodology, R.B., D.C., C.B.C, C.I.D.Z.; Software, R.B.; Investigation, R.B., D.C., C.B.C.; Formal Analysis, R.B., D.C.; Resources, C.I.D.Z.; Writing - Original Draft, R.B., D.C., C.B.C.; Writing – Review & Editing: R.B., D.C., C.B.C., C.I.D.Z.; Visualization, R.B., D.C.; Supervision, C.B.C., C.I.D.Z.; Project Administration, R.B., D.C., C.B.C., C.I.D.Z.; Funding Acquisition, C.I.D.Z.

Declaration of interests

The authors declare no competing interests.

Table 1. Electrophysiological properties of neurons recorded in awake mice.

Group	Side	ID	V_m rest (mV)	Spike amp (mV)	Spike HW (ms)	Rs (MΩ)	Rm (MΩ)	Cm (pF)	Mem constant (τ; ms)
Naive	Ipsi	1	-76.39	24.21	0.49	63.05	52.56	73.87	2.12
	Ipsi	2	-62.16	27.51	0.93	29.15	184.07	21.65	0.54
	Ipsi	3	-58.23	27.66	1.00	37.71	179.21	44.24	1.38
	Ipsi	4	-66.19	51.75	1.33	30.20	854.75	16.98	0.50
	Contra	5	-49.01	48.88	0.98	20.57	1733.81	23.26	0.47
	Contra	6	-62.2	25.31	0.93	51.81	73.50	51.70	1.57
Mean ± SD			**-53.83 ± 9.02**	**34.2 ± 12.6**	**0.94 ± 0.27**	**38.7 ± 15.9**	**513.0 ± 668.1**	**38.6 ± 22.1**	**1.1 ± 0.69**
Cond	Ipsi	1	-43.9	29.54	0.3	43.05	68.31	75.84	2.00
	Ipsi	2	-65.96	36.78	0.99	43.74	474.39	3.49	0.14
	Ipsi	3	-42.59	23.94	0.76	73.64	547.48	7.70	0.50
	Ipsi	4	-46.55	35.31	0.48	36.40	174.57	161.01	4.85
	Contra	5	-72.86	21.96	0.96	37.12	1015.51	18.74	0.67
	Contra	6	-57.51	38.87	2.1	39.56	800.78	2.71	0.10
	Contra	7	-44.78	18.16	0.47	61.24	247.40	485.63	N/A
	Contra	8	-69.78	22.2173	1.08	42.61	382.92	5.02	0.19
Mean ± SD			**-55.49 ± 12.62**	**28.3 ± 7.87**	**0.89 ± 0.56**	**47.17 ± 13.2**	**463.9 ± 320.4**	**95.0 ± 167.2**	**1.21 ± 1.74**

References

1. Gormezano, I., Schneiderman, N., Deaux, E. & Fuentes, I. Nictitating Membrane: Classical Conditioning and Extinction in the Albino Rabbit. *Science* **138**, 33–34 (1962).
2. Schneiderman, N., Fuentes, I. & Gormezano, I. Acquisition and Extinction of the Classically Conditioned Eyelid Response in the Albino Rabbit. *Science* **136**, 650–652 (1962).
3. Jirenhed, D.-A., Bengtsson, F. & Hesslow, G. Acquisition, Extinction, and Reacquisition of a Cerebellar Cortical Memory Trace. *Journal of Neuroscience* **27**, 2493–2502 (2007).
4. Mauk, M. D. & Donegan, N. H. A model of Pavlovian eyelid conditioning based on the synaptic organization of the cerebellum. *Learning & Memory* **4**, 130–158 (1997).
5. Mauk, M. D., Steinmetz, J. E. & Thompson, R. F. Classical conditioning using stimulation of the inferior olive as the unconditioned stimulus. *Proceedings of the National Academy of Sciences* **83**, 5349–5353 (1986).
6. Andersson, G. & Oscarsson, O. Projections to lateral vestibular nucleus from cerebellar climbing fiber zones. *Experimental Brain Research* **32**, (1978).
7. Brodal, P., Dietrichs, E. & Walberg, F. Do pontocerebellar mossy fibres give off collaterals to the cerebellar nuclei? An experimental study in the cat with implantation of crystalline HRP-WGA. *Neuroscience Research* **4**, 12–24 (1986).
8. De Zeeuw, C. I., Van Alphen, A. M., Hawkins, R. K. & Ruigrok, T. J. H. Climbing fiber collaterals contact neurons in the cerebellar nuclei that provide a GABAergic feedback to the inferior olive. *Neuroscience* **80**, 981–986 (1997).
9. Kitai, S. T., McCrea, R. A., Preston, R. J. & Bishop, G. A. Electrophysiological and horseradish peroxidase studies of precerebellar afferents to the nucleus interpositus anterior. I. climbing fiber system. *Brain Research* **122**, 197–214 (1977).
10. van der Want, J. J. L., Wiklund, L., Guegan, M., Ruigrok, T. & Voogd, J. Anterograde tracing of the rat olivocerebellar system with phaseolus vulgaris leucoagglutinin (PHA-L). Demonstration of climbing fiber collateral innervation of the cerebellar nuclei. *The Journal of Comparative Neurology* **288**, 1–18 (1989).
11. Albus, J. S. A theory of cerebellar function. *Math. Biosci.* **10**, 25–61 (1971).
12. Ekerot, C.-F. & Kano, M. Long-term depression of parallel fibre synapses following stimulation of climbing fibres. *Brain Research* **342**, 357–360 (1985).
13. Ito, M. *The Cerebellum and Neural Control*. (New York: Raven Press, 1984).
14. Marr, D. A theory of cerebellar cortex. *J. Physiol.* **202**, 437–470 (1969).
15. Schonewille, M. *et al.* Purkinje Cell-Specific Knockout of the Protein Phosphatase PP2B Impairs Potentiation and Cerebellar Motor Learning. *Neuron* **67**, 618–628 (2010).

16. Ten Brinke, M. M. *et al.* Evolving Models of Pavlovian Conditioning: Cerebellar Cortical Dynamics in Awake Behaving Mice. *Cell Reports* **13**, 1977–1988 (2015).
17. Boele, H.-J. *et al.* Impact of parallel fiber to Purkinje cell long-term depression is unmasked in absence of inhibitory input. *SCIENCE ADVANCES* 9 (2018).
18. Johansson, F., Carlsson, H. A. E., Rasmussen, A., Yeo, C. H. & Hesslow, G. Activation of a Temporal Memory in Purkinje Cells by the mGluR7 Receptor. *Cell Reports* **13**, 1741–1746 (2015).
19. Gao, Z. *et al.* Excitatory Cerebellar Nucleocortical Circuit Provides Internal Amplification during Associative Conditioning. *Neuron* **89**, 645–657 (2016).
20. Boele, H.-J., Koekkoek, S. K. E., De Zeeuw, C. I. & Ruigrok, T. J. H. Axonal Sprouting and Formation of Terminals in the Adult Cerebellum during Associative Motor Learning. *Journal of Neuroscience* **33**, 17897–17907 (2013).
21. Berthier, N. E. & Moore, J. W. Cerebellar Purkinje cell activity related to the classically conditioned nictitating membrane response. *Experimental brain research* **63**, 341–350 (1986).
22. McCormick, D. A. & Thompson, R. F. Neuronal responses of the rabbit cerebellum during acquisition and performance of a classically conditioned nictitating membrane-eyelid response. *The Journal of neuroscience* **4**, 2811–2822 (1984).
23. Ohmae, S. & Medina, J. F. Climbing fibers encode a temporal-difference prediction error during cerebellar learning in mice. *Nature Neuroscience* **18**, 1798–1803 (2015).
24. Ten Brinke, M. M. *et al.* Dynamic modulation of activity in cerebellar nuclei neurons during pavlovian eyeblink conditioning in mice. *eLife* **6**, (2017).
25. Morcuende, S., Delgado-García, J.-M. & Ugolini, G. Neuronal Premotor Networks Involved in Eyelid Responses: Retrograde Transneuronal Tracing with Rabies Virus from the Orbicularis Oculi Muscle in the Rat. *J Neurosci* **22**, 8808–8818 (2002).
26. Pacheco-Calderón, R., Carretero-Guillén, A., Delgado-García, J. M. & Gruart, A. Red Nucleus Neurons Actively Contribute to the Acquisition of Classically Conditioned Eyelid Responses in Rabbits. *J. Neurosci.* **32**, 12129–12143 (2012).
27. Berthier, N. E. & Moore, J. W. Activity of deep cerebellar nuclear cells during classical conditioning of nictitating membrane extension in rabbits. *Experimental brain research* **83**, 44–54 (1990).
28. Clark, G. A., McCormick, D. A., Lavond, D. G. & Thompson, R. F. Effects of lesions of cerebellar nuclei on conditioned behavior and hippocampal neuronal responses. *Brain Research* **291**, 125–136 (1984).
29. Lavond, D. G., Hembree, T. L. & Thompson, R. F. Effect of kainic acid lesions of the cerebellar interpositus nucleus on eyelid conditioning in the rabbit. *Brain Research* **326**, 179–182 (1985).

30. Yeo, C. H., Hardiman, M. J. & Glickstein, M. Classical conditioning of the nictating membrane of the rabbit. I. Lesions of the cerebellar nuclei. *Experimental Brain Research* **60**, 87–98 (1985).
31. Ohyama, T., Nores, W. L., Medina, J. F., Riusech, F. A. & Mauk, M. D. Learning-Induced Plasticity in Deep Cerebellar Nucleus. *Journal of Neuroscience* **26**, 12656–12663 (2006).
32. Medina, J. F., Garcia, K. S. & Mauk, M. D. A Mechanism for Savings in the Cerebellum. *The Journal of Neuroscience* **21**, 4081–4089 (2001).
33. Uusisaari, M. & De Schutter, E. The mysterious microcircuitry of the cerebellar nuclei. *The Journal of Physiology* **589**, 3441–3457 (2011).
34. Uusisaari, M., Obata, K. & Knopfel, T. Morphological and Electrophysiological Properties of GABAergic and Non-GABAergic Cells in the Deep Cerebellar Nuclei. *Journal of Neurophysiology* **97**, 901–911 (2007).
35. Canto, C. B., Witter, L. & De Zeeuw, C. I. Whole-Cell Properties of Cerebellar Nuclei Neurons In Vivo. *PloS one* **11**, e0165887 (2016).
36. Yarden-Rabinowitz, Y. & Yarom, Y. *In vivo* analysis of synaptic activity in cerebellar nuclei neurons unravels the efficacy of excitatory inputs. *The Journal of Physiology* (2017) doi:10.1113/JP274115.
37. Gong, S., DeCuypere, M., Zhao, Y. & LeDoux, M. S. Cerebral cortical control of orbicularis oculi motoneurons. *Brain Research* **1047**, 177–193 (2005).
38. Suzuki, Y., Kiyosawa, M., Mochizuki, M., Ishiwata, K. & Ishii, K. The Pre-Supplementary and Primary Motor Areas Generate Rhythm for Voluntary Eye Opening and Closing Movements. *Tohoku J. Exp. Med.* **222**, 97–104 (2010).
39. Freeman, J. H. & Steinmetz, A. B. Neural circuitry and plasticity mechanisms underlying delay eyeblink conditioning. *Learning & Memory* **18**, 666–677 (2011).
40. Nicholson, D. A. & Freeman, J. H., Jr. Selective Developmental Increase in the Climbing Fiber Input to the Cerebellar Interpositus Nucleus in Rats. *Behavioral Neuroscience* **118**, 1111–1116 (2004).
41. McCormick, D. A. & Thompson, R. F. Cerebellum: Essential involvement in the classically conditioned eyelid response. *Science* **223**, 296–299 (1984).
42. Sugihara, I. & Shinoda, Y. Molecular, Topographic, and Functional Organization of the Cerebellar Nuclei: Analysis by Three-Dimensional Mapping of the Olivonuclear Projection and Aldolase C Labeling. *Journal of Neuroscience* **27**, 9696–9710 (2007).
43. Hioki, H. *et al.* Differential distribution of vesicular glutamate transporters in the rat cerebellar cortex. *Neuroscience* **117**, 1–6 (2003).

44. Krueger-Burg, D., Papadopoulos, T. & Brose, N. Organizers of inhibitory synapses come of age. *Current Opinion in Neurobiology* **45**, 66–77 (2017).
45. Tyagarajan, S. K. & Fritschy, J.-M. Gephyrin: a master regulator of neuronal function? *Nat Rev Neurosci* **15**, 141–156 (2014).
46. Uusisaari, M. & Knöpfel, T. Functional Classification of Neurons in the Mouse Lateral Cerebellar Nuclei. *The Cerebellum* **10**, 637–646 (2011).
47. De Zeeuw, C. I. & Berrebi, A. S. Postsynaptic Targets of Purkinje Cell Terminals in the Cerebellar and Vestibular Nuclei of the Rat. *European Journal of Neuroscience* **7**, 2322–2333 (1995).
48. Celio, M. R. Calbindin D-28k and parvalbumin in the rat nervous system. *Neuroscience* **35**, 375–475 (1990).
49. Scotti, A. L. Calbindin D28k in the olivocerebellar projection. A light and electron microscope study. *J Anat* **187**, 649–659 (1995).
50. Eccles, J. C., Ito, M. & Szentagothai, J. *The cerebellum as a neuronal machine*. (Springer, New York, 1967).
51. Leergaard, T. B. & Bjaarlie, J. G. Topography of the complete corticopontine projection: From experiments to principal maps. *Frontiers in Neuroscience* **1**, 211–223 (2007).
52. Bracha, V., Webster, M. L., Winters, N. K., Irwin, K. B. & Bloedel, J. R. Effects of muscimol inactivation of the cerebellar interposed-dentate nuclear complex on the performance of the nictitating membrane response in the rabbit. *Experimental brain research* **100**, 453–468 (1994).
53. Freeman, J. H. & Rabinak, C. A. Eyeblink conditioning in rats using pontine stimulation as a conditioned stimulus. *Integrative Physiological & Behavioral Science* **39**, 180–191 (2004).
54. Freeman, J. H., Halverson, H. E. & Poremba, A. Differential Effects of Cerebellar Inactivation on Eyeblink Conditioned Excitation and Inhibition. *Journal of Neuroscience* **25**, 889–895 (2005).
55. Lavond, D. G. & Steinmetz, J. E. Acquisition of classical conditioning without cerebellar cortex. *Behavioral Brain Research* **33**, 113–164 (1989).
56. Mojtahedian, S., Kogan, D. R., Kanzawa, S. A., Thompson, R. F. & Lavond, D. G. Dissociaton of conditioned eye and limb responses in the cerebellar interpositus. *Physiology & Behavior* **91**, 9–14 (2007).
57. Sears, L. L. & Steinmetz, J. E. Acquisition of classically conditioned-related activity in the hippocampus is affected by lesions of the cerebellar interpositus nucleus. *Behavioral neuroscience* **104**, 681 (1990).
58. Sears, L. L. & Steinmetz, J. E. Dorsal accessory inferior olive activity diminishes during acquisition of the rabbit classically conditioned eyelid response. *Brain Research* **545**, 114–122 (1991).

59. Wikgren, J. & Korhonen, T. Interpositus nucleus inactivation reduces unconditioned response amplitude after paired but not explicitly unpaired treatment in rabbit eyeblink conditioning. *Neuroscience letters* **308**, 181–184 (2001).
60. Freeman, J. H., Carter, C. S. & Stanton, M. E. Early cerebellar lesions impair eyeblink conditioning in developing rats: differential effects of unilateral lesions on postnatal day 10 or 20. *Behavioral neuroscience* **109**, 893 (1995).
61. Clark, R. E., Lavond, D. G. & Zhang, A. A. Reversible lesions of the cerebellar interpositus nucleus during acquisition and retention of a classically conditioned behavior. *Behavioral Neuroscience* **106**, 879–888 (1992).
62. Heiney, S. A., Wojaczynski, G. J. & Medina, J. F. Action-based organization of a cerebellar module specialized for predictive control of multiple body parts. *Neuron* **109**, 2981-2994.e5 (2021).
63. Foscarin, S. *et al.* Experience-Dependent Plasticity and Modulation of Growth Regulatory Molecules at Central Synapses. *PLoS ONE* **6**, e16666 (2011).
64. Zheng, N. & Raman, I. M. Synaptic Inhibition, Excitation, and Plasticity in Neurons of the Cerebellar Nuclei. *The Cerebellum* **9**, 56–66 (2010).
65. Koekkoek, S. K. E., Den Ouden, W. L., Perry, G., Highstein, S. M. & De Zeeuw, C. I. Monitoring kinetic and frequency-domain properties of eyelid responses in mice with magnetic distance measurement technique. *Journal of neurophysiology* **88**, 2124–2133 (2002).
66. Heiney, S. A., Wohl, M. P., Chettih, S. N., Ruffolo, L. I. & Medina, J. F. Cerebellar-Dependent Expression of Motor Learning during Eyeblink Conditioning in Head-Fixed Mice. *Journal of Neuroscience* **34**, 14845–14853 (2014).
67. Paxinos, G. & Franklin, K. B. J. *The Mouse Brain in Stereotaxic Coordinates*. (Gulf Professional Publishing, 2004).
68. Witter, L., Canto, C. B., Hoogland, T. M., de Gruijl, J. R. & De Zeeuw, C. I. Strength and timing of motor responses mediated by rebound firing in the cerebellar nuclei after Purkinje cell activation. *Frontiers in Neural Circuits* **7**, (2013).

492 **Online Methods**

493 **Animals and ethics statement**

494 All animal experimental procedures were conducted in accordance with the institutional animal
495 welfare committees of the Erasmus Medical Center, Rotterdam, and/or the Royal Dutch Academy of
496 Arts and Sciences, Amsterdam, and adhered to the European guidelines for the care and use of
497 laboratory animals (Council Directive 86/6009/EEC). Adult male and female C57Bl/6J mice (4-12 weeks
498 old, institutional colony and from Janvier Laboratories) were socially housed in a 12-h light and dark
499 cycle with *ad libitum* access to food and water.

500

501 **Surgical methods**

502 *Pedestal surgery*

503 Mice were anesthetized with isoflurane (5% induction, 1.8-2% maintenance; in 0.2 L/min O_2 and 0.2
504 L/min air) and placed in a stereotaxic frame where their body temperature was kept at 37 °C using a
505 feedback-controlled heating-pad. Eyes were covered with antimicrobial ointment (Terra-Cortril,
506 Pfizer) to prevent drying. Skin covering the skull was shaved and a mid-sagittal incision of
507 approximately 1 cm was made to expose the skull bone, after which local anesthesia was applied on
508 the skin around the incision (10% Xylocaine, AstraZeneca). Primer (Optibond All-In-One, Kerr) was
509 applied on the bone and treated with UV light. A 6 x 3 x 5.7 mm aluminum block ('pedestal') was
510 attached to a stereotaxic arm for correct positioning, and attached to the skull bone with dental acrylic
511 (Flowline, Heraeus Kulzer). Skin edges were attached to the dental acrylic using tissue glue (Histoacryl,
512 Aesculap). Post-operative analgesia was given subcutaneously with Meloxicam (2 mg/kg Metacam,
513 Boehringer Ingelheim Animal Health) and mice were placed under an infrared light while recovering
514 from anesthesia. Mice recovered for at least two days following surgery before subsequent
515 experiments.

516

517 *Viral injections and optic fiber surgery*

518 Mice were prepared for surgery as described above. A longer mid-sagittal incision was made until the
519 edge of the occipital bone. Aa stereotaxic arm was used to mark the location of entry to reach the
520 lateral pontine nuclei (PN) (-3.8 to -4 mm from bregma, ± 1 mm lateral to midline, -5.5 to -5.8 mm
521 depth), comparable to previously used coordinates[20]. Two small craniotomies were made using a
522 dental drill (Foredom Drill K1070-2E, Blackstone Industries) and the dura was carefully removed using
523 a fine forceps (Dumont #5). Mice were injected with AAV1/Syn-Chronos-GFP (UNC Vector Core, lot
524 #AV6550). Final concentration was diluted 4x and a total of 1 µL virus solution was injected in each
525 hemisphere using borosilicate glass pipettes connected to a Nanoject II Auto-Nanoliter Injector (2

µL/min, Drummond Scientific). The pipette was left in place for at least 2 minutes to allow diffusion and was then slowly retracted. Bilateral optic fibers (Ø200 µm, FT200UMT, Thorlabs) connected to ceramic zirconia ferrules (MM-FER2007C-2300, Precision Fiber Products) were lowered into the brain through the same injection track until a depth of 5 mm was reached to enable light delivery to the PN. Fibers were attached to the skull bone using primer and dental cement, after which pedestals were attached on the skull. Dental cement was painted using silver conductive paint (RS Components) to reduce the escape of optogenetic light. Mice were allowed to recover at least 2 weeks before subsequent experiments.

Craniotomy surgery

Mice were prepared for surgery as described above. Eyes were protected and kept moist using eye drops (Duodrops, Ceva Santé Animale). Hairs in the neck were removed and an incision was made in the skin covering the neck muscles, after which local anesthesia was applied (10% Xylocaine, AstraZeneca). Neck muscles were removed to expose the occipital bone and two square-shaped bilateral craniotomies were made using a dental drill. Position of craniotomy was above Crus II to access the CN in a 43° angle. A thin layer of primer was applied around the craniotomies and a recording bath was made using dental acrylic (Flowline and Charisma, Heraeus Kulzer). The recording bath was filled with 0.9% NaCl solution to keep the dura moist. Skin and muscles surrounding the bath were attached to the dental cement using tissue glue. The dura in the craniotomy was carefully removed using a needle tip (30G x ½ inch, Microlance, BD) and fine forceps (Dumont #7 curved). Directly after removing the dura, the recording bath was cleaned with 0.9% NaCl solution and filled with a low viscosity silicone elastomer sealant (Kwik-cast, World Precision Instruments,) to protect the brain tissue from the air. Mice were given post-operative analgesia subcutaneously (Metacam 2 mg/kg) and were placed under an infrared light during recovery. Mice were closely monitored for at least two hours before starting the recording session.

Eyeblink conditioning

Habituation

Mice were habituated for 3-5 days before starting EBC trainings. Habituations and trainings were done in sound- and light-isolating boxes (Neurasmus) equipped with a cylindrical treadmill and a horizontal bar for head fixation[66]. Eyelid movements were measured using magnet distance measuring technique (MDMT)[65] or using a high-speed camera[24]. In both cases, mice were shortly anesthetized with isoflurane (5% in 0.5 L/min O_2 and 0.5 L/min air) and placed on the treadmill after which they woke

559 up in the dark environment of the box. Mice were habituated with increasing durations ranging from
560 15 min on day 1 to 60 min on day 5.
561 For habituations with MDMT, the left eye of the mouse was prepared over the course of
562 habituations. Hairs under the left eyelid were removed under isoflurane anesthesia on day 2. From
563 day 3 onward a 1.5 x 0.5 x 0.7 mm neodymium magnet (Supermagnete) was placed under the left eye
564 using super glue (Bison International). Eyelid movements were recorded through a magnetic sensor
565 that was placed above the left eye. During the habituation session, 20 CS trials and 2 US trials with an
566 inter-trial-interval (ITI) between 10-12 ± 2 sec were presented to familiarize the mouse with the
567 stimuli. The CS consisted of a 260 ms light flash delivered through a green/blue LED placed ~7 cm in
568 front of the mouse. The US consisted of a 10 ms corneal air puff (35-40 psi) delivered through a P20
569 pipette tip positioned ~5 mm from the left eye. The US airflow was controlled by a Milli-Pulse Pressure
570 Injector (MPPI-3, Applied Scientific Instrumentation). CS and US stimuli were identical in camera
571 boxes, but no magnet sensor was present. Mice were placed in the camera boxes without isoflurane
572 anesthesia. They also did not undergo shaving of the hairs under the eyelid or magnet placement.
573
574 *Acquisition trainings*
575 Acquisition trainings lasted 5-10 days and consisted of one training session daily. A session was
576 comprised of 200 CS-US (paired) trials, 20 CS trials and 20 US trials, presented as a 20x repeated block
577 of 1US-10paired-1CS. Trials followed a standardized format of 0-500 ms baseline, 500-760 ms CS
578 (paired and CS trials), 750-760 ms US (paired and US trials), 760-2000 ms post-stimuli period. MDMT
579 data was captured at 1017.26 Hz using custom-written LabVIEW software (National Instruments)[65].
580 Trainings were started at least 10 min after placing mice in the box to allow full recovery of isoflurane
581 anesthesia. Trials were initiated only if the eye was >75% opened.
582
583 *Eyeblink conditioning during electrophysiology*
584 Mice for *in vivo* extracellular and whole-cell recordings were first trained in boxes using MDMT, after
585 which they were transferred to an electrophysiology setup equipped with a camera. Mice were then
586 trained for at least 3 more days on this setup before performing recording sessions, to ensure they
587 reached maximum performance. A 250 fps CCD camera (scA640-120gc, Basler) was directed at the left
588 eye, which was illuminated with an infrared light. Camera frames were transformed into a data vector
589 based on pixel thresholding within a region of interest overlaying the eye and the eyelid. The resulting
590 data was sampled at 2441 Hz. Stimuli were triggered under the control of custom-made software
591 utilizing TDT System 3 (Tucker Davis Technologies) and NI-PXI (National Instruments) processors.
592 During the US the TTL onset was corrected for the delay between TTL onset and air puff arrival at the

cornea (13 ms). Trials were initiated only if the eye was >75% opened. To avoid distortion of the camera signal caused by reflection of the infrared light from the whiskers, a thin layer of water-proof black mascara was applied on the left whiskers before mice were positioned in the setup. Timings and parameters of stimuli were identical to those used during the acquisition training sessions.

Eyeblink data processing and quantification

MDMT data was processed using custom LabVIEW software (Neurasmus). Acquired data was subjected to several quality checks: (i) trials with an unstable baseline were removed (trials with values exceeding 5x SD during the baseline period) and (ii) sessions with a large variation in UR amplitude (>0.5 x CV) were excluded. Finally, sessions from which more than 75% of trials was removed were excluded to ensure accurate behavioral measurements. CRs were defined as eyelid closures during the last 200 ms of the CS-US interval that exceeded 10% of UR amplitude. UR amplitude was calculated as the average of full eyelid closures during US only trials. Camera data was analyzed using custom-made MATLAB scripts. Acquired data was preprocessed by filtering with a Gaussian low-pass filter (50 Hz cutoff frequency) and trials with unstable baselines (values >5 x SD of the baseline period) were excluded. CRs were defined as eyelid closures during the last 200 ms of the CS-US interval that exceeded 5 x SD of values during the baseline period.

CR percentage was calculated by dividing the number of CR+ trials by the total amount of eligible CR trials, multiplied by 100%. CR amplitude was calculated by dividing the maximum eyelid closure during the CS-US interval by the average UR amplitude, multiplied by 100%. CR amplitude at US onset represents the amplitude of eyelid closure at US onset (750 ms after trial start), divided by the average UR amplitude, multiplied by 100%. CR or EO onsets were manually detected on a trial-by-trial basis in a blind manner. They are defined as the time value of the last minimum (CR) or last maximum (EO) before a continuously rising (CR) or decreasing (EO) signal.

Microelectrode stimulation and Evans Blue labeling

Before starting the electrophysiological recording part of the study we determined the recording location. Microelectrode stimulation was performed to induce eyelid movements using an 80-µm-diameter platinum iridium monopolar electrode (100 KΩ; Alpha Omega) lowered into the brain with a 43° angle until a depth of 1500-1600 µm was reached. Electrodes were advanced in steps of 100 µm while currents were generated (ISO-flex Stimulus Isolater, A.M.P.I.) in the range of 1–15 µA (200 ms pulse trains; 250 µs biphasic pulses; 500 Hz). The depth at which reliable eyelid contractions could be observed with low current amplitudes (<10 µA) was identified as the eyeblink-encoding region of the CN. To mark this area in the CN, the electrode was retracted, coated with Evans Blue solution (5% in

627 saline, Sigma-Aldrich) and reinserted using identical position and coordinates. Mice were
628 transcardially perfused using 4% paraformaldehyde (PFA, Sigma-Aldrich) in phosphate buffered saline
629 (PBS) after a lethal dose of pentobarbital (Nembutal) and brains were collected for histology.
630
631 ***In vivo* electrophysiology**
632 Whole-cell and extracellular recordings were made using glass electrodes with a tip diameter of 1-2
633 µm and a resistance of 4-8 MΩ. Electrodes were heat-pulled on a P-1000 micropipette puller (Sutter
634 Instrument) from filamented borosilicate glass capillaries (1.5 mm OD, 0.86 mm ID, Harvard
635 Apparatus). Electrodes were back-filled with intracellular solution, containing (in mM): 10 KOH, 3.48
636 $MgCl_2$, 4 NaCl, 129 K-Gluconate, 10 HEPES, 17.5 glucose 4 Na_2ATP, and 0.4 Na_3GTP (295 - 305 mOsm;
637 pH 7.2). The intracellular solution was supplemented with 0.5% Neurobiotin (Vector Labs).
638 Electrophysiological recordings were made using a Multiclamp 700B amplifier (Axon Instruments,
639 Molecular Devices) and digitized at 100 or 50 kHz with a Digidata 1440 digitizer (Axon Instruments).
640 Electrodes were mounted with a 43° angle on a pipette holder connected to a head stage (CV-7B, Axon
641 Instruments). Pipette movements were controlled by a micromanipulator (SM7, Luigs und Neumann,
642 Ratingen, GE). Pipettes were targeted at the IntA and DLH region of the cerebellar nuclei and entered
643 the surface of the cerebellum in a 43° angle at the following coordinates: 1.5-2.0 mm lateral and -1.5
644 mm below Bregma, as previously described[35]. Electrodes were advanced high pressure to a depth of
645 1500-1600 µm relative to the brain surface, after which the pressure was lowered to 15-20 mbar.
646 During whole-cell recordings, electrodes were advanced in steps of 2 µm while monitoring the
647 current during 10 mV steps at 33 Hz in voltage clamp mode. All neurons reached a seal resistance of
648 at least 1 GΩ before establishing whole-cell configuration. Several protocols were run shortly after
649 break-in to characterize the neuron, including a sealtest protocol (10 mV steps at -65 mV) and a
650 current step protocol (200 to -200 pA) in current clamp mode after compensation. Following these
651 protocols, continuous recordings were made without current injection in current clamp mode while
652 CS, US and CS-US paired trials were given (naive animals: 1:1:1 ratio in pseudorandomized order,
653 conditioned animals: repetitive sequences of 1US-5paired-1CS to maintain conditioned behavior
654 throughout the experiment). Trial ITI was 12 ± 2 s and no threshold for eyelid opening was used to
655 maximize the number of trials. Camera recordings of the eyelid were made simultaneously. Recordings
656 were made until the neuron was lost or the recording quality became insufficient. Only one recordings
657 session was performed following the craniotomy surgery. During extracellular recordings, electrodes
658 were advanced until action potentials (>1 mV) of a single neuron could be identified. Then, CS, US and
659 CS-US trials were given while spiking responses were recorded. Awake whole-cell recordings were

made during only 1 session with a duration of <4 hours. Extracellular recordings were made during 1-3 daily sessions each with a duration of <4 hours.

Data analysis electrophysiology

Data was processed in Clampfit (v10.5, Axon Instruments) and MATLAB (R2011b and R2022a, MathWorks). Access resistance (R_a) and membrane resistance (R_m) were estimated based on the peak amplitude of average current signal and the amplitude of the relaxation phase during a 10 mV voltage step, respectively. Membrane time constant (tau) was estimated by fitting a single exponential function on the average current signal between 80-10% of peak-to-relaxation amplitude of the same voltage step. Data of recordings during EBC were imported in MATLAB and synchronized with eyelid recordings based on TTL timings. For analysis of the V_m spikes were removed by median filtering (10 ms window). Trial data was separated based on trial type and eyelid response. Traces were normalized to the baseline (250-500 ms) of the trial. CS-evoked responses were obtained by averaging paired and CS only trials up until the US onset (0-750 ms). Threshold for detecting significant V_m responses (EPSPs or IPSPs) was 3x SD of the baseline. EPSP amplitude and peak time were determined for individual trials and averaged per neuron. EPSP onsets were manually and blindly determined on a trial-by-trial basis and were defined as the time point of the last minimum before a continuously increasing signal.

Spikes were detected using a custom-written MATLAB spike analysis program (B.H.J. Winkelman, Netherlands Institute for Neuroscience, Amsterdam), after which spikes were sorted based on spike waveform characteristics. Only data with spikes from single units were included in the analysis. Based on spike times we calculated: spiking frequency (= number of spikes / duration of time period) and coefficient of variation of spiking (CV = standard deviation (all inter-spike-intervals (ISIs) / average (all ISIs)). Spikes in V_m recordings were detected using a Clampfit threshold search and spontaneous spike calculations were based on periods of quiet wakefulness directly after the start of recording, before the first stimulus was presented. For extracellular data, time periods between trials were used.

Exclusion and quality criteria whole-cell recordings

Recordings were discarded if R_a exceeded 100 MΩ or if spike amplitudes were lower than 10 mV. Neurons were identified based on occurrence of clear spikes (spontaneous or current-induced). Only good traces with a non-drifting V_m were selected for further analysis. Although neurons were generally recorded without current injection, few neurons received limited current (-25 to -200 pA) to maintain V_m at original values directly after break-in. Neurons were recorded in both hemispheres (naive: 4/6 ipsilateral; conditioned: 4/8 ipsilateral) and we did not find a relation between laterality and CS-

evoked V_m amplitude (P = 0.636, unpaired t-test). Recording depth (1794.9 ± 54.25 µm) was consistent with the depth of the CN[35,67].

Optogenetics

Mice used for optogenetic experiments were trained for 10 days in EBC and subjected to optogenetic stimulation sessions on day 0, 5 and 10. Bilateral optogenetic activation of PN neurons was achieved by 465 nm light-induced activation of Chronos. Light was generated by a 5W LED (60 lm, LZ1-B200, LED Engin Inc.) connected to a custom-made LED driver, as described previously[68]. This resulted in a light output of 1-2.5 mW at the tip of the optic fiber implants. LEDs were controlled by TTL pulses from the amplifier. Timings of TTL pulses was used to synchronize electrophysiology and camera recordings. Silver conductive paint and aluminum foil coating was used to reduce the escape of optogenetic light from the fibers and equipment. The area under the curve (AUC) for the eyelid responses was calculated as the absolute sum of the normalized-to-baseline eyelid trace 0-150 ms after LED onset.

Histological procedures

Mice were deeply anesthetized with pentobarbital (Nembutal) and transcardially perfused with 100 ml 4% paraformaldehyde (PFA) in 0.12 M phosphate buffer. Brains were dissected and post-fixed overnight at 4°C, then cryoprotected in 0.12 M phosphate buffer containing 30% sucrose at 4°C until they sank. Cerebella were cut on a cryostat into 25 µm-thick coronal or sagittal sections and collected in phosphate-buffered saline (PBS). Primary antibodies were incubated overnight at 4°C in PBS containing 0.25% Triton X-100, and 5% fetal calf serum. Primary antibodies were: mouse anti-NeuN (1:500, Millipore), chicken anti-GFP (1:700, Aves Labs), mouse anti-calbindin (1:1500, Swant), rabbit anti-VGLUT1 (1:1000, Synaptic Systems), guinea pig anti-VGLUT2 (1:1000, Synaptic Systems), mouse anti-gephyrin (1:500, Synaptic Systems). After washing, sections were then incubated for 1 h at room temperature with one of the following fluorophore-conjugated secondary antibodies or streptavidin: donkey anti-mouse Cy3 (ThermoFisher Scientific), goat anti-chicken Alexa Fluor 488 (ThermoFisher Scientific), donkey anti-guinea pig Cy3 (ThermoFisher Scientific), donkey anti-rabbit Alexa Fluor 647 (ThermoFisher Scientific), streptavidin-488 (ThermoFisher Scientific), streptavidin-Cy3 (Jackson Immunoresearch). For each immunohistochemical reaction, slices from all experimental conditions were processed together and incubation times kept constant. After processing sections were mounted on microscope slides with Tris-glycerol supplemented with 10% Mowiol (Merck Millipore Calbiochem).

Imaging

Fluorescent images were acquired using a confocal microscope (SP5 and SP8, Leica Microsystems). Confocal images were taken at a resolution of 1024 x 1024 dpi and a 50 Hz speed. Laser intensity, gain and offset were maintained constant in each analysis. Quantitative evaluations were made by a blind experimenter using Image J software. Adobe Photoshop 6.0 (Adobe Systems) was used to adjust image contrast and assemble the final plates.

Quantification of density of glutamatergic terminals

To estimate the density of VGLUT1 and VGLUT2-positive axon terminals, at least three coronal sections containing the DLH or the IntA (Bregma: -6.00, -6.12 µm) were selected for each animal (pseudoconditioned mice, N = 6; conditioned mice, N = 4). A 0.5 µm-thick confocal image/side in each section was captured under a 63x objective. The ''analyze particle'' function of ImageJ was used to estimate the density of boutons (number of terminals/mm^2) in each image, after selecting the automatic threshold to remove unwanted background information.

Quantification of gephyrin-positive puncta

Single 0.4 µm thick-confocal images of the DLH or the IntA (right and left side) in coronal sections (Bregma: -6.00, -6.12) have been collected under a 63x objective with 2.5x zoom. At least three sections have been selected/mouse. On such images the density of gephyrin-positive puncta around the soma of excitatory neurons (identified by their size, *i.e.* > 240 μm^{34}) has been evaluated by Image J and expressed as number/µm neuronal membrane (pseudoconditioned mice, N = 6; DHL, n = 110 neurons; IntA, n = 100 neurons; conditioned mice, N = 4; DLH right side, n = 53 neurons, DLH left side, n = 31 neurons; IntA right side, n = 37 neurons, IntA left side, n = 25 neurons). For each neuron the number of gephyrin-positive puncta that did not face a calbindin-positive terminal was quantified and the % of those puncta (out of the total number of puncta) was calculated.

Decoding analysis

Decoding (10 fold cross-validation) was performed on pooled trial data and therefore a varying number of trials for each neuron. For whole-cell data decoding was performed on spike-removed, normalized and Gaussian filtered (10 ms) V_m traces. For spike data, spikes were binned into 5 ms time intervals, Gaussian filtered (25 ms) and normalized to baseline rate. The dataset was then divided in a train and test set (9:1 ratio) and decoding was performed using the *classify* function in MATLAB (custom MATLAB code by M. Tang, Australian National University, 2022). Accuracy represents the percentage of accurately classified trials for each sampling point or time bin.

Statistics

Statistical analysis was carried out using MATLAB (R2011b and R2022a, MathWorks, CA, USA), SPSS (v22, IBM, NY, USA), GraphPad Prism 5 and 9 (GraphPad Software Inc., CA, USA). Normality of distributions was assessed using Shapiro-Wilk test and. Homogeneity of variance was assessed using Bartlett's test. If the assumption of normality was violated, non-parametric alternatives were performed. Behavioral performance was analyzed using a repeated-measures ANOVA or linear mixed models (if missing data) with the maximum likelihood method. Group and session/day was modelled as fixed effects, and %CR and FEC at US onset were modelled as dependent variables. We assessed the fit of the model by running the analysis with the unstructured, diagonal and first-order autoregressive repeated covariance types, after which we choose the covariance type with the lowest Akaike's information criterion (AIC) value. This was often the unstructured covariance type. Data is reported as mean ± standard error of the mean (s.e.m), unless indicated otherwise. Data is shown in figures as mean ± s.e.m., unless indicated otherwise. $P < 0.05$ was considered to be statistically significant. To test whether the decoder performed above chance level, we performed a cluster-corrected permutation test with 2000 permutations in MATLAB (E. Spaak, Oxford University, 2015).

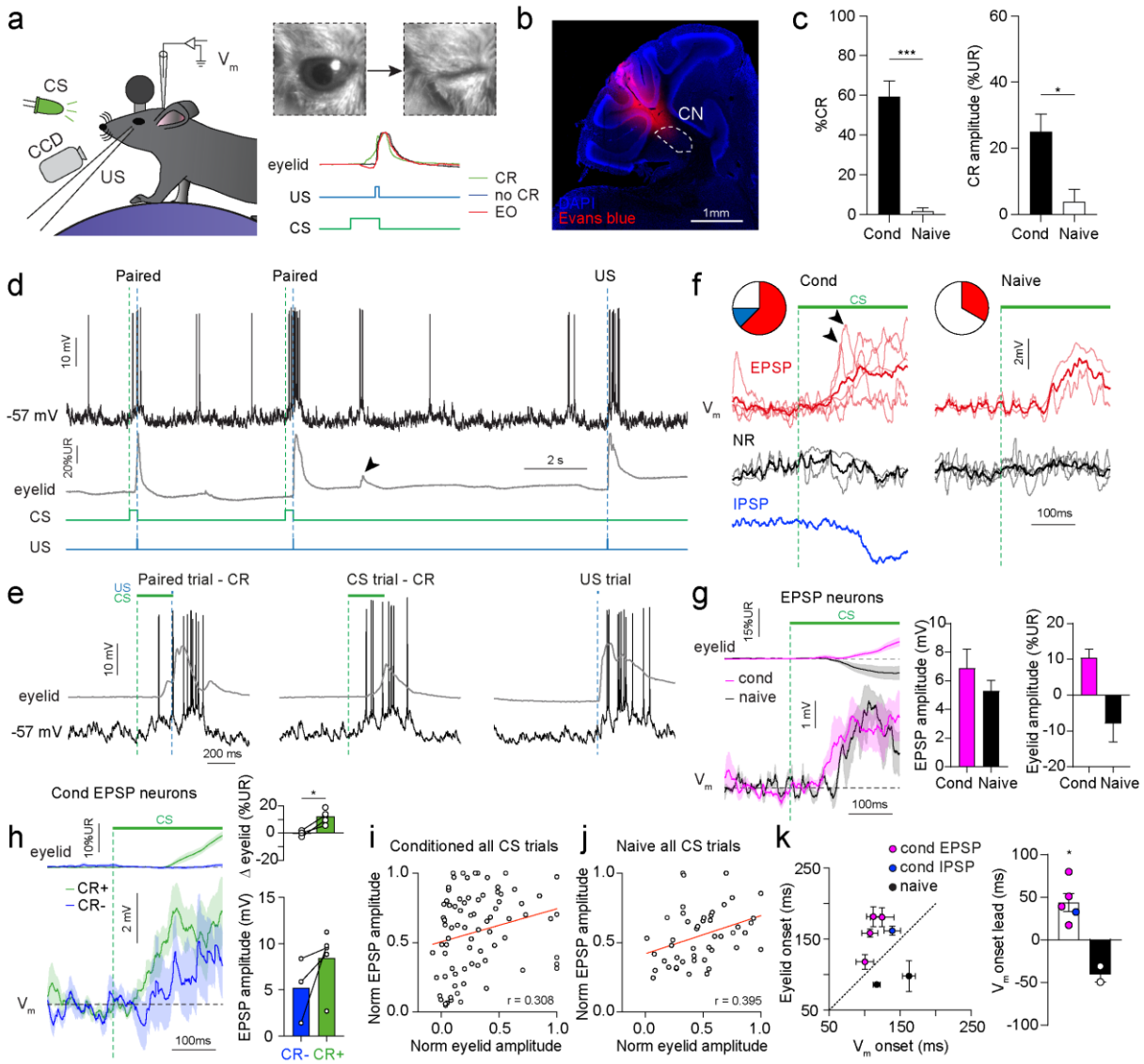

Fig. 1. Membrane potential encoding of the conditioned stimulus in CN neurons. a, Schematic of *in vivo* whole-cell recordings of head-fixed mice on a treadmill during EBC. Eyelid responses to CS and US stimuli are recorded using a camera. Upward deflections in the eyelid trace indicate eyelid closures, downward deflections indicate eyelid openings. CR: conditioned response, EO: eyelid opening. **b**, Recordings were targeted at the CN. Electrode track is visualized by coating the electrode with Evans blue dye. **c**, Performance of conditioned and naive mice during the recordings. Conditioned mice showed a higher %CR (59.4 ± 22.7% vs 1.67 ± 4.08%, $P < 0.001$, Mann-Whitney U test (MWT)) and CR amplitude (25.1 ± 14.9 vs 3.80 ± 9.32 %UR, $P = 0.01$, MWT). **d,e**, Example trace (**d**) and CS-US paired, CS only and US only trial traces (**e**) with eyelid movements. CN neuron shows excitatory post-synaptic potentials (EPSPs) and spike activity following the CS and US, and during spontaneous eyelid closures (arrowhead). **f**, Average CS responses of all neurons in conditioned (n = 8 neurons) and naive (n = 6 neurons) mice. Neurons were classified as EPSP, no response (NR) or inhibitory post-synaptic potential

(IPSP) neurons. Arrow heads indicate early EPSP peak specific to conditioned neurons. **g**, Average traces from EPSP neurons with eyelid movements for conditioned (n = 5 neurons) and naive (n = 2 neurons) mice. Conditioned mice showed eyelid closures (10.35 ± 2.50 %UR), whereas naive mice showed eyelid openings (EO) (-7.87 ± 5.21 %UR). EPSP amplitudes were comparable (cond: 6.86 ± 3.05 mV, naive: 5.30 ± 1.03 mV). **h**, Average traces from EPSP neurons in conditioned mice, separated between CR+ (n = 5 neurons) and CR- trials (n = 3 neurons). CRs only took place during CR+ trials (*P* = 0.046, paired t-test). EPSP amplitudes during CR+ and CR- trials were comparable (CR+: 8.42 ± 3.32 vs CR-: 5.22 ± 3.53 mV, *P* = 0.194, paired t-test). **i**, Correlation analysis across all trials of conditioned EPSP neurons (n = 79 trials/5 neurons, r = 0.308, *P* = 0.006, Spearman) and naive EPSP neurons (**j**, n = 47 trials/2 neurons, r = 0.395, *P* = 0.006, Spearman) comparing EPSP amplitude versus eyelid movement amplitude. **k**, V_m onset versus eyelid movement onset for conditioned and naive mice (CR for cond, EO for naive mice). V_m onset (116.74 ± 6.79 ms) leads CR onset (160.04 ± 11.57 ms) in conditioned mice (*P* = 0.0136, one-sample t-test). In naive mice, V_m onset (139.8 ± 32.08 ms) follows eyelid onset (91.88 ± 8.53 ms). All data are represented as mean ± s.e.m.

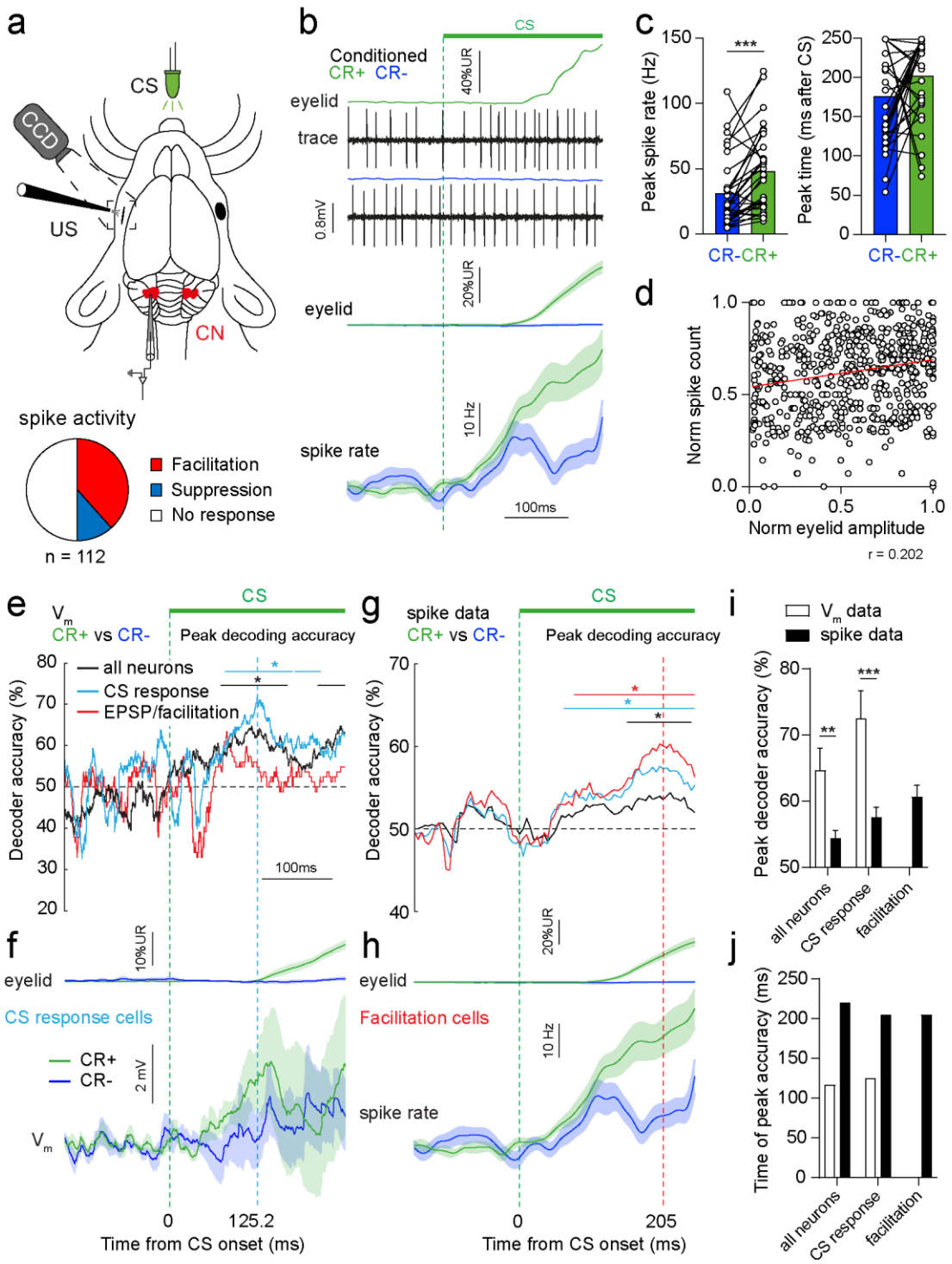

806

807 **Fig. 2. Spike activity and decoding of neuronal activity underlying eyelid movements. a**, Schematic
808 of *in vivo* juxtasomal recordings from CN neurons in head-fixed mice on a treadmill during EBC. **b**,
809 Example spike facilitation neuron showing increased spike activity coinciding with a CR (top). Average
810 of all spike facilitation neurons (n = 30) showing eyelid movements on CR+ and CR- trials with
811 normalized spike rates (bottom). **c**, Average peak spike rates on CR- and CR+ trials. Significantly higher
812 spike rates are observed during CR+ trials (CR+: 48.22 ± 5.80 Hz vs CR-: 31.12 ± 4.95 Hz, $P < 0.001$,

Wilcoxon), but the time of peak spike rate after CS onset is comparable (CR+: 202.6 ± 9.98 ms vs CR-: 176.2 ± 11.43 ms, P = 0.083, Wilcoxon). **d**, Pooled correlation analysis of all CR+ trials (n = 648/30 neurons) shows a significant association between number of spikes during the CS-US interval and CR amplitude (r = 0.202, P < 0.001, Spearman). **e**, Decoding of CR+ versus CR- trial based on pooled V_m data from conditioned mice. Decoding was significantly above chance when including all neurons (n = 8, peak accuracy: 64.68 ± 3.30% at 117.06 ms after CS onset) and CS-responding neurons (n = 6, 72.46 ± 4.24% at 125.2 ms after CS onset), but not for EPSP neurons. **f**, Average V_m trace on CR+ and CR- trials for CS-responding neurons. Time of peak decoding accuracy coincides with CR onset. **g**, Decoding of CR+ versus CR- trial based on pooled spike data from conditioned mice. Decoding was significantly above chance when including all neurons (n = 112, peak accuracy: 54.41 ± 1.16 ms at 220 ms after CS onset) and CS-responding neurons (n = 56, peak accuracy: 57.67 ± 1.46 ms at 220 ms after CS onset), but performed best when including spike facilitation neurons (n = 30, peak accuracy: 60.65 ± 1.74 ms at 220 ms after CS onset). **i**, Peak decoding accuracy was significantly higher for Vm data compared to spike data when including all neurons (P = 0.004, MWT) and CS-responders (P < 0.001, MWT). **j**, Time of peak accuracy comparing V_m and spike data. All data is represented as mean ± s.e.m.

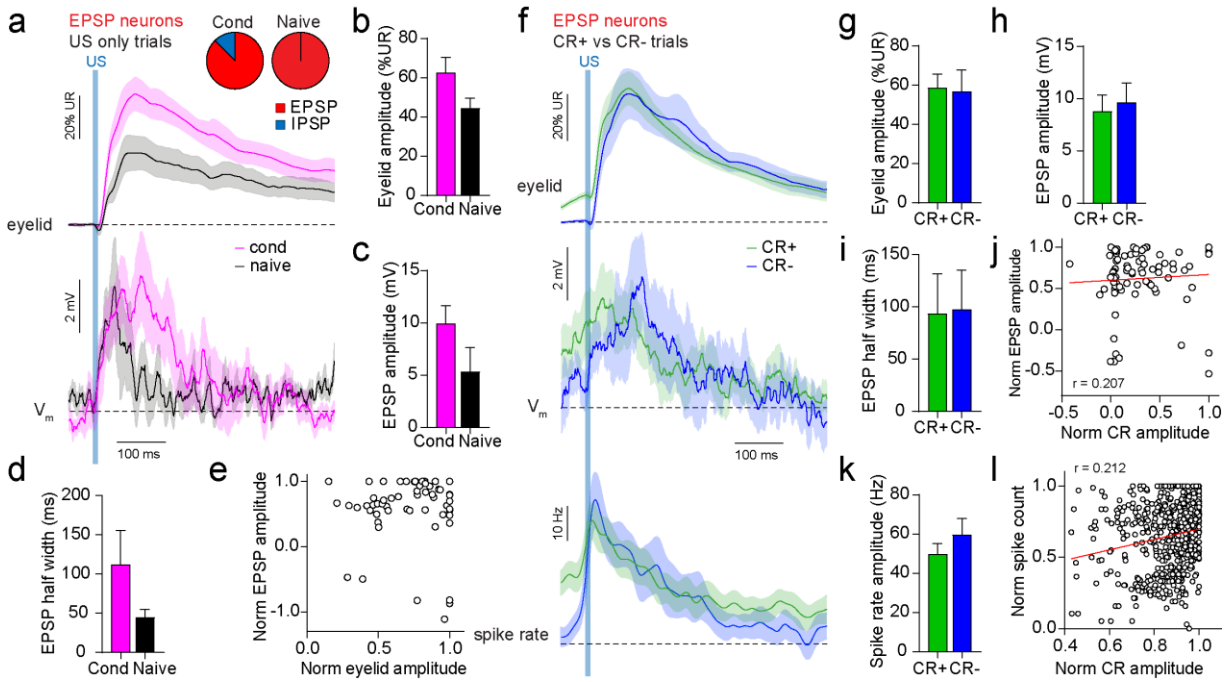

Fig. 3. Membrane potential dynamics and spike coding during the unconditioned stimulus. a, Eyelid closures and EPSP responses during US only trials. All conditioned (n = 8, 87.5% EPSP, 12.5% IPSP) and naive (n = 6, 100% EPSP) neurons responded to the US. Amplitude of eyelid closure (**b**, P = 0.105, independent t-test), EPSP amplitude (**c**, P = 0.123, independent t-test) and EPSP half width (**d**, P = 0.201, Welch's t-test) were not significantly different between groups. **e**, Correlation analysis between normalized eyelid and EPSP amplitude did not reveal a significant relation (r = 0.03, P = 0.422, Spearman). **f**, Average eyelid, V_m and spike rate traces for EPSP neurons (n = 6) and spike facilitation neurons (n = 33), separating CR+ and CR- trials on CS-US paired trials of conditioned mice. Eyelid amplitude (**g**, P = 0.728, paired t-test), EPSP amplitude (**h**, P = 0.997, paired t-test), and EPSP half width (**i**, P = 0.759, paired t-test) were comparable. **j**, Correlation analysis between normalized CR amplitude and US-evoked EPSP amplitude revealed a significant relation (r = 0.207, P = 0.031, Spearman). **k**, US-evoked spike rate amplitude was comparable between CR+ and CR- trials (P = 0.135, Wilcoxon). **l**, Correlation analysis between normalized CR amplitude and spike count following the US revealed a significant relation (r = 0.212, P < 0.001, Spearman). All data is represented as mean ± s.e.m.

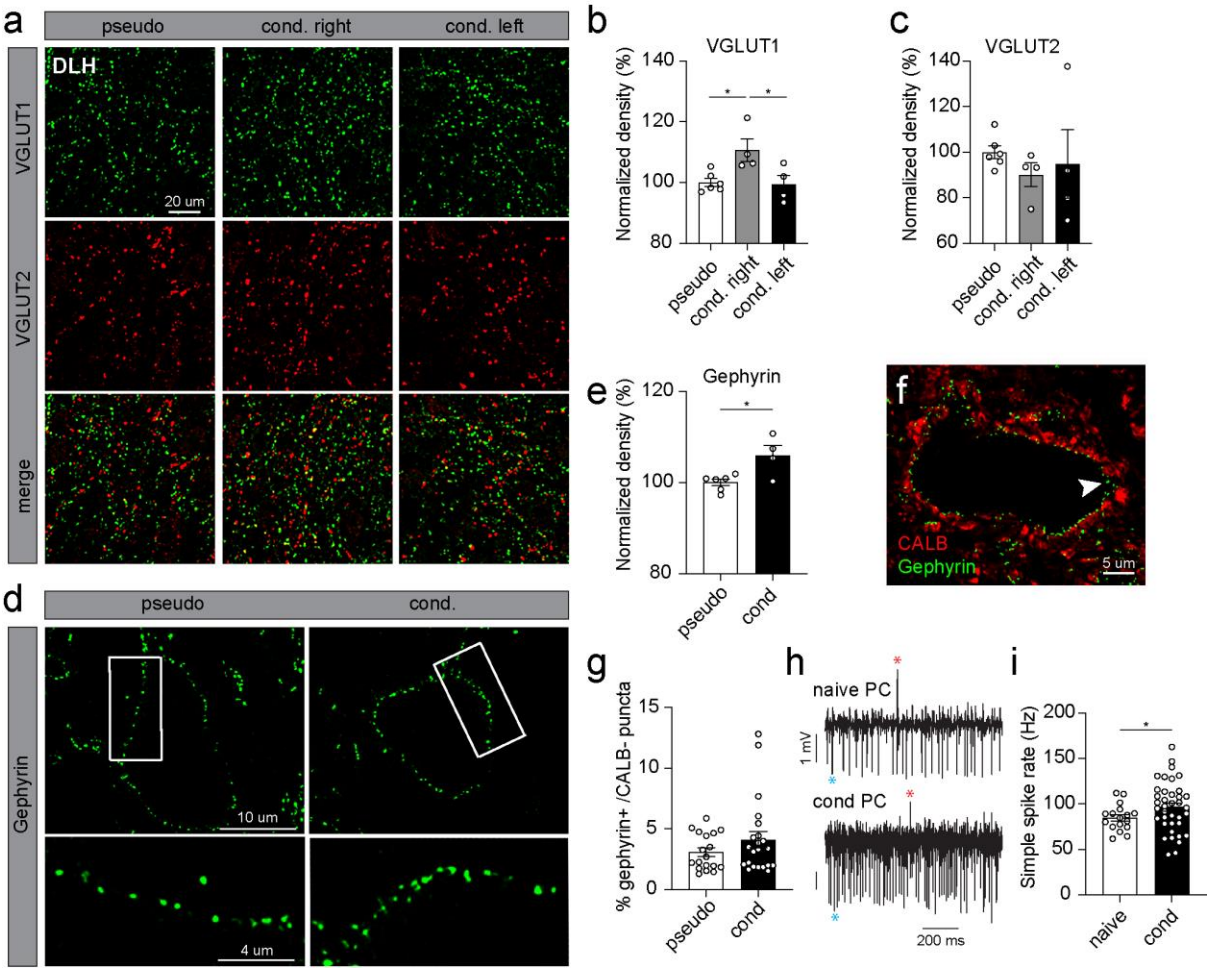

Fig. 4. Changes in VGLUT1+ MF terminals, PC terminals and PC simple spike activity. a, Expression of VGLUT1 and 2 in the DLH of conditioned mice (n = 4), separating the left and right hemisphere, and in pseudoconditioned (pseudo) mice (n = 6). **b**, Density of VGLUT1 puncta was significantly higher in conditioned mice in the DLH of the right hemisphere (contralateral to air puff) (cond. right: 110.63 ± 3.63% normalized to pseudo, *P* = 0.018, ANOVA, cond. right vs pseudo p = 0.026, Turkey), but not in the left hemisphere (cond. left: 99.41 ± 2.96%; cond. left vs right p = 0.031, Tukey). **c**, Density of VGLUT2 puncta in the DLH was unchanged after conditioning (*P* = 0.678, ANOVA). **d**, Expression of Gephyrin in the DLH of conditioned and pseudo mice. **e**, Conditioned mice show a significantly higher Gephyrin density (105.95 ± 2.22%, *P* = 0.016, independent t-test). **f**, Expression of CALB and Gephyrin around a putative glutamatergic DLH neuron. **g**, Quantification of Gephyrin+/CALB- couples (non-PC inhibitory inputs) revealed no difference between conditioned and pseudo mice (pseudo, n = 30 neurons; cond., n = 35 neurons, *P* = 0.431, MWT). **h**, Traces of PCs in lobule HVI in conditioned and naive mice showing simple spikes (blue asterisk) and complex spikes (red asterisk). **I**, Spontaneous simple spike rate was higher in conditioned mice (n = 38, 96.7 ± 4.50 Hz) compared to naive PCs (n = 17, 84.8 ± 3.50 Hz, *P* = 0.043, Welch's t-test). All data is represented as mean ± s.e.m.

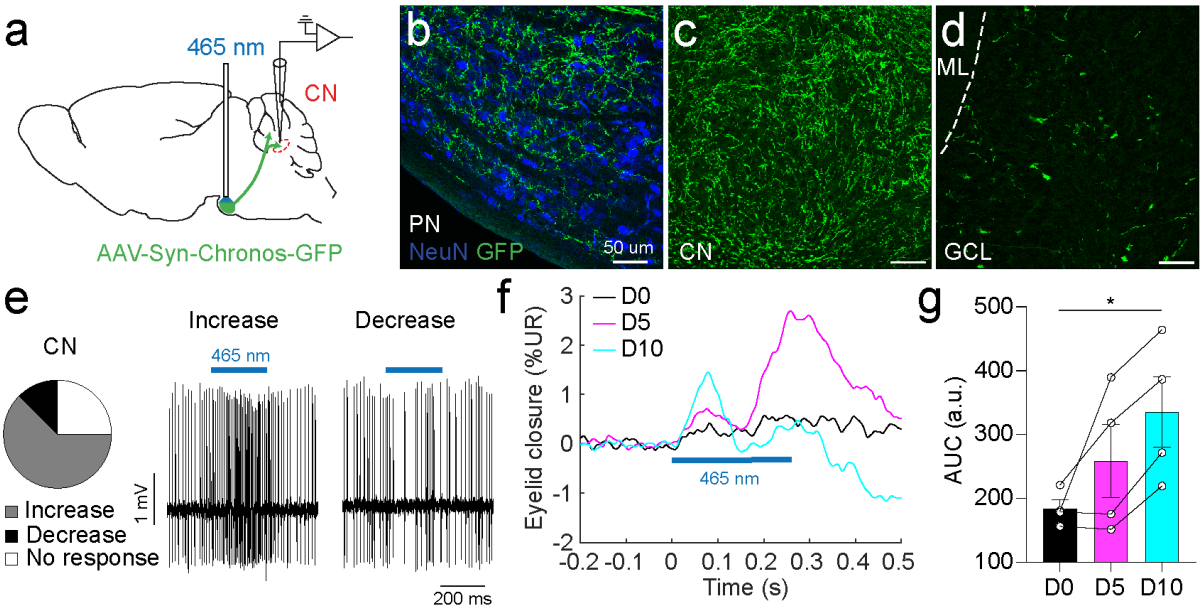

Fig. 5. Optogenetic activation of PN neurons evokes larger eyelid movements after conditioning. a, Schematic of optogenetic stimulation of pontine nuclei neurons giving rise to MFs targeting the cerebellum. AAV-Chronos-GFP was injected bilaterally in the PN and optic fiber implants were placed. Expression of GFP in the PN (**b**), CN (**c**) and granule cell layer (GCL). **d**, confirmed expression in MFs. No expression was seen in the molecular layer (ML) indicating that no CFs were labeled. **e**, Juxtasomal loose-patch recordings (n = 24) confirmed bidirectional modulation of activity during optogenetic stimulation (62% increased, 13% decreased spike rate). **f**, Average eyelid movements of mice (n = 4) during optogenetic stimulation of PN neurons on day (D) 0, D5 and D10 of conditioning. **g**, Area under the curve (AUC) of short-latency eyelid movements (0-150 ms after LED onset) show an significant increase during training (AUC at D0 vs D5 vs D10: 184.2 ± 13.57 vs 258.9 ± 57.1 vs 335.7 ± 55.31, *P* = 0.028, RM ANOVA, D0 vs D10: p = 0.023, Tukey). All data is represented as mean ± s.e.m.

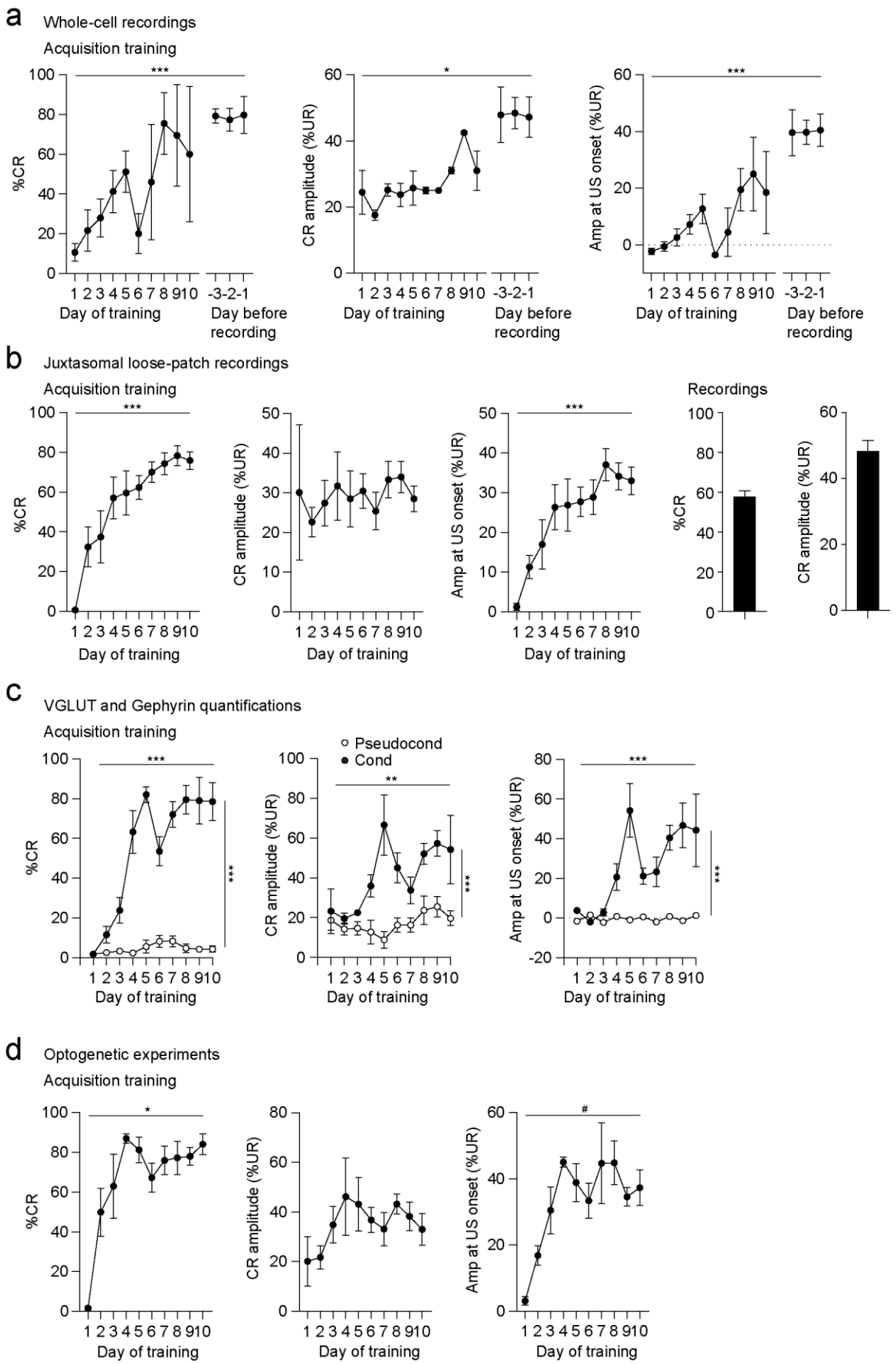
a
Whole-cell recordings
Acquisition training
%CR
CR amplitude (%UR)
Amp at US onset (%UR)
Day of training
Day before recording
b
Juxtasomal loose-patch recordings
Acquisition training
Recordings
c
VGLUT and Gephyrin quantifications
Acquisition training
Pseudocond
Cond
d
Optogenetic experiments
Acquisition training

877 **Supplementary Fig. 1. Learning curves of conditioned and pseudoconditioned mice in this study. a**,
878 Conditioned mice for *in vivo* awake whole-cell recordings (n = 7 mice, n = 2 mice day 6-10) showed
879 robust learning during acquisition training as an increasing %CR ($P < 0.001$, linear mixed model (LMM)),
880 CR amplitude ($P = 0.013$, LMM) and eyelid amplitude at US onset ($P < 0.001$, LMM). After training mice
881 were placed in the electrophysiology setup and trained for >3 days to maintain high levels of
882 performance (day before recording). **b**, Conditioned mice for juxtasomal loose-patch recordings (n =
883 8) showed an increasing %CR ($P < 0.001$, LMM) and eyelid amplitude at US onset ($P < 0.001$, LMM).
884 CRs occurred in 57.95 ± 2.67% of trials during recordings and had amplitudes of 48.38 ± 3.1 %UR. **c**,
885 Training performance of conditioned (n = 4) and pseudoconditioned mice (n=6) for quantification of
886 VGLUT1, VGLUT2 and Gephyrin. Pseudoconditioned mice received the same number of stimuli as
887 conditioned mice, but unpaired. Conditioned mice showed learning whereas pseudoconditioned mice
888 did not (day, group and day*group interaction effects for %CR, CR amplitude and eyelid amplitude at
889 US onset all have $P < 0.002$, LMM). Day 5 of training was followed by two days without training, which
890 explains the temporary decrease in performance. **d**, Conditioned mice for optogenetic experiments (n
891 = 4) showed increasing %CR ($P = 0.013$, one-way repeated measures (RM) ANOVA) and a trend towards
892 an increasing eyelid amplitude at US onset ($P = 0.056$, RM ANOVA). All data is represented as mean ±
893 s.e.m.
894

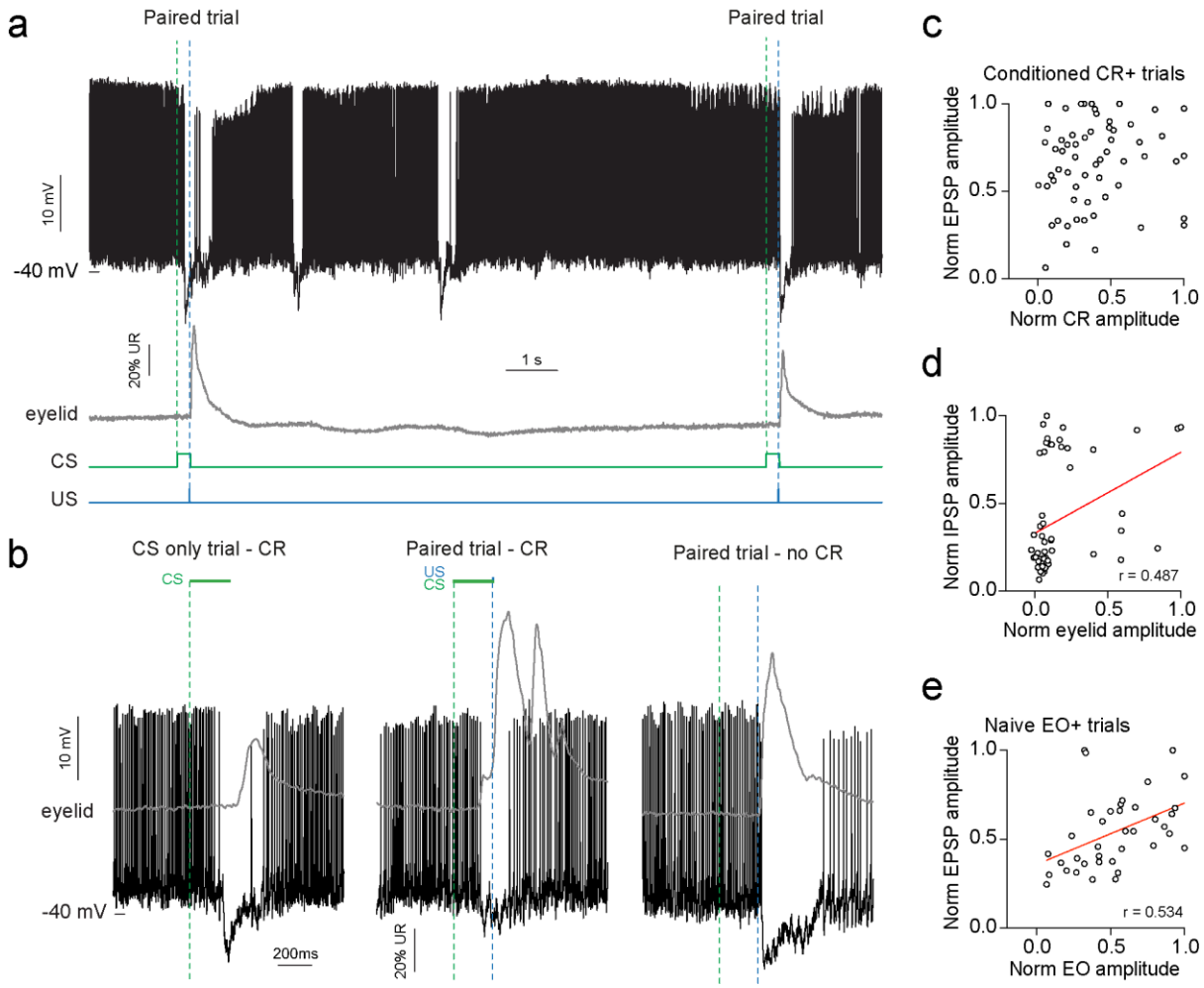

Supplementary Fig. 2. Example IPSP neuron and correlations between V_m dynamics and eyelid movements. a,b, Example trace (**a**) and CS only, CS-US paired with CR and CS-US paired without CR (**b**) with respective eyelid movements. CN neuron shows inhibitory post-synaptic potentials (IPSPs) and reductions in spike activity following the CS and US, associated with the occurrence of a CR. **c**, Correlation analysis across CR+ trials of conditioned EPSP neurons (n = 60 trials/5 neurons, r = 0.219, *P* = 0.161, Spearman). **d**, Correlation analysis across all CS trials of one conditioned IPSP neuron (n = 57 trials/1 neuron, r = 0.487, *P* < 0.001, Spearman). **e**, Correlation analysis across EO+ trials in naive EPSP neurons (n = 38 trials/2 neurons, r = 0.534, *P* < 0.001, Spearman) comparing EPSP amplitude versus eyelid movement amplitude. All data is represented as mean ± s.e.m.

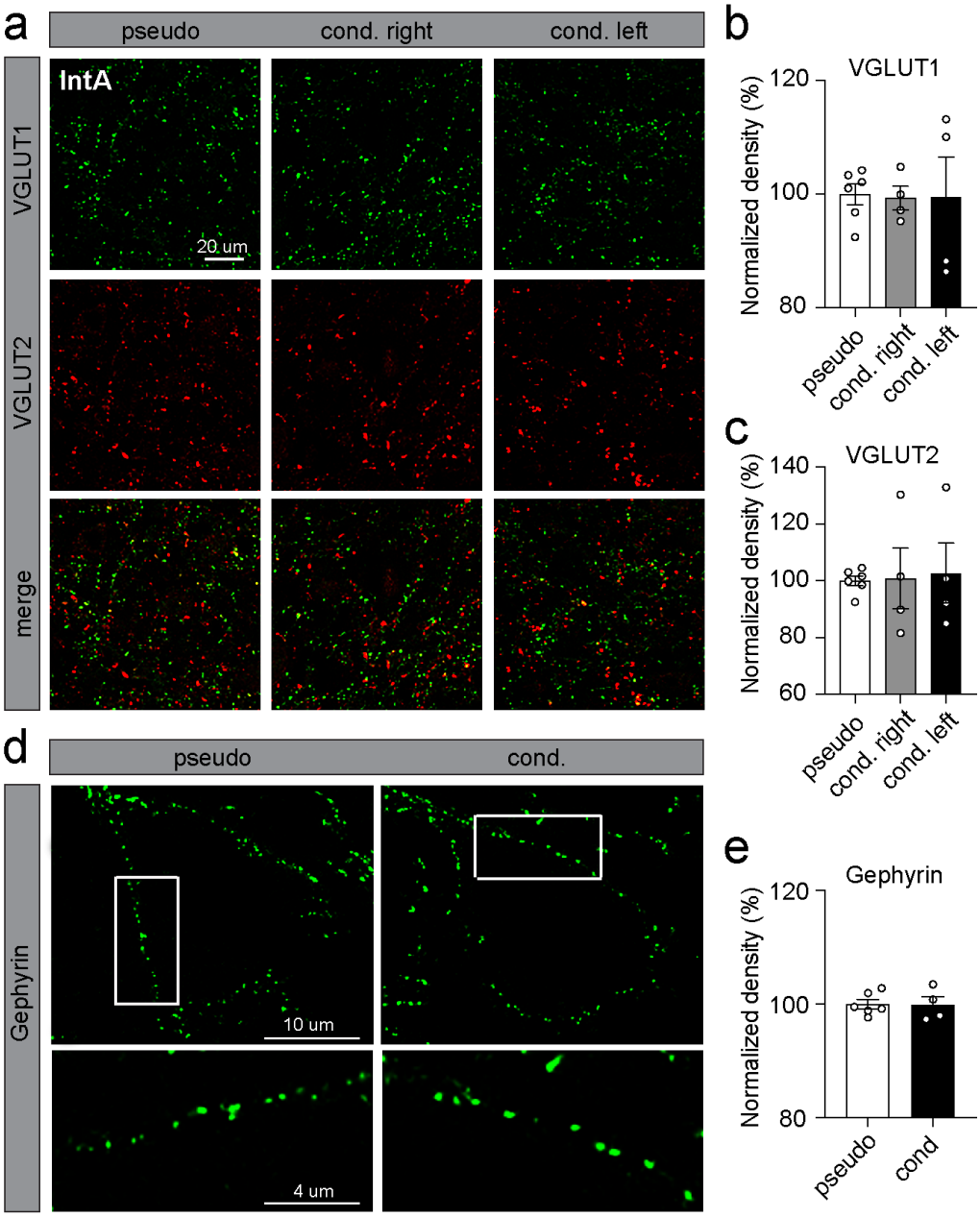

Supplementary Fig. 3. VGLUT1, VGLUT2 and Gephyrin expression in the IntA. a, Expression of VGLUT1 and 2 in the IntA of conditioned mice (n = 4), separating the left and right hemisphere, and in pseudoconditioned (pseudo) mice (n = 6). Densities of VGLUT1 puncta (**b**) and VGLUT2 puncta (**c**) in the IntA were comparable between conditioned and pseudoconditioned mice (VGLUT1: $P = 0.990$, VGLUT2: $P = 0.966$, ANOVA). **d**, Expression of Gephyrin in the IntA of conditioned and pseudo mice. **e**, Conditioned and pseudo mice showed comparable densities of Gephyrin density ($P = 0.952$, independent t-test;). All data is represented as mean ± s.e.m.